Calhoun: The NPS Institutional Archive

DSpace Repository

Theses and Dissertations | 1. Thesis and Dissertation Collection, all items

1989-12

Characterization of the corrosion of a P-130x graphite fiber reinforced 6063 aluminum metal matrix composite.

King, Joel David

Monterey, California. Naval Postgraduate School

http://hdl.handle.net/10945/25734

This publication is a work of the U.S. Government as defined in Title 17, United States Code, Section 101. Copyright protection is not available for this work in the United States.

Downloaded from NPS Archive: Calhoun

http://www.nps.edu/library

Calhoun is the Naval Postgraduate School's public access digital repository for research materials and institutional publications created by the NPS community. Calhoun is named for Professor of Mathematics Guy K. Calhoun, NPS's first appointed -- and published -- scholarly author.

Dudley Knox Library / Naval Postgraduate School
411 Dyer Road / 1 University Circle
Monterey, California USA 93943

NAVAL POSTGRADUATE SCHOOL
Monterey, California

THESIS

K435

CHARACTERIZATION OF THE CORROSION OF A
P-130X GRAPHITE FIBER REINFORCED
6063 ALUMINUM METAL MATRIX COMPOSITE

by

Joel David King

December 1989

Thesis Advisor Indranath Dutta

Approved for public release; distribution is unlimited.

T247936

REPORT DOCUMENTATION PAGE

1a Report Security Classification Unclassified			1b Restrictive Markings
2a Security Classification Authority			3 Distribution Availability of Report
2b Declassification Downgrading Schedule			Approved for public release; distribution is unlimited.
4 Performing Organization Report Number(s)			5 Monitoring Organization Report Number(s)
6a Name of Performing Organization Naval Postgraduate School	6b Office Symbol *(if applicable)* 34		7a Name of Monitoring Organization Naval Postgraduate School
6c Address *(city, state, and ZIP code)* Monterey, CA 93943-5000			7b Address *(city, state, and ZIP code)* Monterey, CA 93943-5000
8a Name of Funding Sponsoring Organization	8b Office Symbol *(if applicable)*		9 Procurement Instrument Identification Number
8c Address *(city, state, and ZIP code)*			10 Source of Funding Numbers
		Program Element No	Project No / Task No / Work Unit Accession No

11 Title *(include security classification)* CHARACTERIZATION OF THE CORROSION OF A P-130X GRAPHITE FIBER REINFORCED 6063 ALUMINUM METAL MATRIX COMPOSITE

12 Personal Author(s) Joel David King

13a Type of Report	13b Time Covered	14 Date of Report *(year, month, day)*	15 Page Count
Master's Thesis	From To	December 1989	90

16 Supplementary Notation The views expressed in this thesis are those of the author and do not reflect the official policy or position of the Department of Defense or the U.S. Government.

17 Cosati Codes			18 Subject Terms *(continue on reverse if necessary and identify by block number)*
Field	Group	Subgroup	Aluminum, Graphite, Metal Matrix Composite, MMC, Corrosion, Electrochemical, Sulfite, pH, Heat Treatment.

19 Abstract *(continue on reverse if necessary and identify by block number)*

The corrosion behavior of a P-130x graphite fiber reinforced 6063 aluminum 0-90 cross plied metal matrix composite was studied. Electrochemical tests were performed on the composite and the monolithic matrix metal in aqueous 3.5% NaCl solutions. Immersion tests were performed on the composite in aqueous 3.5% NaCl solutions. The effects of pH, the presence of sulfite ions, and various heat treatments were investigated. The electrochemical tests included studies of galvanic corrosion, corrosion potential, galvanostaircase cyclic polarization and polarization resistance.

Immersion tests showed accelerated corrosion at the exposed interfaces, with preferential attack at transverse fiber layers. Galvanic corrosion was large at low pH values, large graphite area fractions and when the matrix was in the over-aged state. The corrosion potential of the composite was found to be electronegative to the monolith when the Gr-Al interfaces were exposed to the electrolyte. Low pH values and over-aging increased pitting susceptibility. Solutionizing and quenching lowered pitting susceptibility at pH 8 but increased it at pH 4. Low pH values, the presence of sulfite ions and over- aging increased general corrosion rates.

20 Distribution Availability of Abstract	21 Abstract Security Classification	
☒ unclassified unlimited ☐ same as report ☐ DTIC users	Unclassified	
22a Name of Responsible Individual Indranath Dutta	22b Telephone *(include Area code)* (408) 646-2851	22c Office Symbol 69Du

DD FORM 1473,84 MAR 83 APR edition may be used until exhausted
All other editions are obsolete

Approved for public release; distribution is unlimited.

Characterization of the Corrosion of a P-130x Graphite Fiber Reinforced 6063 Aluminum Metal Matrix Composite

by

Joel David King
Lieutenant, United States Navy
B.S., Rensselaer Polytechnic Institute, 1982

Submitted in partial fulfillment of the
requirements for the degree of

MASTER OF SCIENCE IN MECHANICAL ENGINEERING

from the

NAVAL POSTGRADUATE SCHOOL
December 1989

ABSTRACT

The corrosion behavior of a P-130x graphite fiber reinforced 6063 aluminum 0-90 cross plied metal matrix composite was studied. Electrochemical tests were performed on the composite and the monolithic matrix metal in aqueous 3.5% NaCl solutions. Immersion tests were performed on the composite in aqueous 3.5% NaCl solutions. The effects of pH, the presence of sulfite ions, and various heat treatments were investigated. The electrochemical tests included studies of galvanic corrosion, corrosion potential, galvanostaircase cyclic polarization and polarization resistance.

Immersion tests showed accelerated corrosion at the exposed interfaces, with preferential attack at transverse fiber layers. Galvanic corrosion was large at low pH values, large graphite area fractions and when the matrix was in the over-aged state. The corrosion potential of the composite was found to be electronegative to the monolith when the Gr-Al interfaces were exposed to the electrolyte. Low pH values and over-aging increased pitting susceptibility. Solutionizing and quenching lowered pitting susceptibility at pH 8 but increased it at pH 4. Low pH values, the presence of sulfite ions and over- aging increased general corrosion rates.

C.1

TABLE OF CONTENTS

I. INTRODUCTION 1

A. CORROSION OF ALUMINUM ALLOYS 4

B. CORROSION OF METAL MATRIX COMPOSITES 8

C. RESEARCH OBJECTIVES AND OVERVIEW 12

II. CORROSION THEORY AND EXPERIMENTAL ELECTROCHEMICAL TECHNIQUES 13

A. CORROSION POTENTIAL 13

B. TAFEL EXTRAPOLATION 15

C. POLARIZATION RESISTANCE 16

D. CYCLIC ANODIC POLARIZATION 17

E. CYCLIC GALVANOSTAIRCASE POLARIZATION 20

F. GALVANIC CORROSION 23

III. EXPERIMENTAL EQUIPMENT AND PROCEDURES 24

A. MATERIALS 24

B. SAMPLE PREPARATION 25

1. Composite and 6063 Monolithic Aluminum 25

2. Graphite Fiber Electrodes 26

C. DATA ACQUISITION EQUIPMENT 28

1. PAR Model K47 Corrosion Cell 28

2. PAR Model 273 Potentiostat / Galvanostat 32

3. PAR Model 351 Corrosion Measurement System 32

a. Safety Considerations 33

D. ELECTROCHEMICAL TECHNIQUE PARAMETERS 33
1. Corrosion Potential Test Parameters 35
2. Tafel Plot Test Parameters 35
3. Polarization Resistance Test Parameters 36
4. Cyclic Galvanostaircase Polarization Test Parameters 36
5. Galvanic Corrosion Test Parameters 37
E. IMMERSION TESTING 37
IV. RESULTS AND SUMMARY 40
A. GALVANIC CORROSION CURRENT RESULTS 40
B. PITTING SUSCEPTIBILITY 43
C. CORROSION CURRENT FROM LINEAR POLARIZATION 50
D. POLARIZATION OF ALUMINUM BY GRAPHITE 58
E. IMMERSION TESTS RESULTS 62
V. CONCLUSIONS 68
VI. RECOMMENDATIONS FOR FUTURE RESEARCH 71
APPENDIX A 73
APPENDIX B 75
APPENDIX C 78
REFERENCES 80

I. INTRODUCTION

A composite is a material formed from two or more constituents combined on a macroscopic scale and designed to feature the best properties of each constituent. The development of composites as engineering materials has been chiefly in response to the demand for structural materials having a combination of properties not found in the monolithic substances already in use. Typical combinations of properties desired include:

- High strength–to–weight ratios.
- High stiffness–to–weight ratios.
- Wear resistance with fracture toughness.
- Low density and high thermal conductivity.
- Strength with corrosion resistance.

Roles in which composites find themselves include those in aircraft, high–speed manufacturing machinery, power–generating equipment, and aerospace equipment. [Ref. 1]

Composite materials generally consist of a bulk material, called the matrix, and a reinforcement of some type. Reinforcements are often particulate or fibrous, and carry a large fraction of the applied stresses. The matrix surrounding the reinforcement enables the transfer of stresses to the reinforcement. The resultant composites can be broadly divided into three groups associated with the matrix material: plastic, metal, and ceramic. [Ref. 2]

Metal–matrix composites are attractive in many applications because the matrix's metallic properties have those advantages which have led metal alloys to the premiere role they play in modern dynamic engineering structures. These include: [Ref. 1]

- High Strength.
- High Moduli
- High toughness and impact properties.
- Low sensitivity to temperature changes.
- Ductility.
- High electrical and thermal conductivity.

The graphite–fiber reinforced aluminum–matrix composites are of interest to both the scientific community and to industry. Aluminum is of interest because of its high strength, ductility, and thermal and electrical conductivities. Graphite fibers are attractive because of their high modulus of elasticity and thermal conductivity. When combined to form a metal matrix composite (MMC), aluminum and graphite yield a new material combining strength, ductility, and high thermal conductivity.

The aluminum alloy 6603 reinforced with 27 volume percent P–130x continuous graphite fibers is being considered as a new material for electronic module frames by the Naval Weapons Support Center, Crane, Indiana because of its low–density, high–stiffness and high–thermal conductivity. The thermal conductivity of the module frame material is of prime importance, as heat removal from electronics is often a limiting design factor.

For a continuous fiber reinforced composite with unidirectional fiber orientation, the composite elastic modulus (E_{comp}) and the composite thermal conductivity (k_{comp}) are give by the rule of mixtures as:

$$E_{comp} = V_m E_m + V_f E_f$$

$$k_{comp} = V_m k_m + V_f k_f$$

where V_m and V_f are the respective metal and fiber volume fractions, E_m and E_f are the respective metal and fiber elastic moduli, and k_m and k_f are the respective metal and fiber thermal conductivities.

Table 1 lists the modulus of elasticity (E) and the coefficient of thermal conductivity (k) of 6063 aluminum, P-130x graphite fibers, and the composite as predicted by the rule of mixtures.

TABLE 1

MODULUI OF ELASTICITY AND

COEFFICIENTS OF THERMAL CONDUCTIVITY

Material	E (GPa)	k (W/°C•m)
Al 6063	68.3	193
P-130x	896	800
Composite	292	357

Combined as a MMC, 6063 aluminum and P–130x graphite fibers have the potential to fulfill the high stiffness and thermal conductivity requirements for advanced electronic module frames.

A. CORROSION OF ALUMINUM ALLOYS

Aluminum alloys are usually covered with a cohesive and tenacious oxide layer, which acts as a protective coating. The oxide layer on aluminum forms immediately upon exposure to the atmosphere and is responsible for aluminum's low general corrosion rate. Aluminum is, however, quite susceptible to localized forms of attack, such as pitting and crevice corrosion, which break down the oxide layer to allow comparatively rapid dissolution of aluminum ions and subsequent rapid corrosion.

Once immersed in water the oxide layer grows, becoming much thicker and porous. Under corrosive conditions, such as in sea water, the oxide layer will cease to grow at some point. A thickness characteristic of the equilibrium between oxide formation and oxide dissolution or breakdown is established. R. A. Bonewitz [Ref. 3] found higher corrosion rates of 6063 aluminum at higher temperatures, and tentatively attributed this to higher oxide dissolution rates. Figure 1 shows the Pourbaix diagram for aluminum. It indicates that for a nominal corrosion potential of -0.78 V, aluminum is more susceptible to corrosion at pH 4 than at pH 8. This may be due to higher oxide dissolution rates at pH 4.

The obvious corrosive element in a marine environment is sea water. The primary solute in sea water is sodium chloride (NaCl), which, along with other salts, constitutes roughly 3.5% of sea water by weight. For this reason, a 3.5% aqueous solution of sodium chloride is often used in laboratory corrosion experiments to simulate sea water. Using the solution of a single salt also limits the number of variables being investigated, and allows better elucidation of the role of a single ionic species.

The naturally occurring elements in sea water are not the only ones of concern in marine corrosion. The exhaust gases, or stack gas, of a naval ship contain various corrosive ingredients. The most important of these are the sulfur oxides, sulfur dioxide (SO_2) and sulfur trioxide (SO_3). Most of the sulfur in the fuel oxidizes to SO_2, which when mixed with moisture forms sulfurous acid. A wide variety of concentrations of the sulfurous acid may be encountered, depending upon the sulfur concentration of the fuel oil, the dilution of the stack gas, etc. [Ref. 4]

Pitting is the most commonly encountered form of aluminum corrosion. In certain near–neutral aqueous solutions a pit once initiated will continue to grow, as the solution within the pit becomes acidic. When the aluminum atoms migrate out of the pits, alumina precipitates as a membrane, further isolating and intensifying pit acidity. [Ref. 5]

M. G. Fontanta [Ref. 6] states that the chloride ions in an aqueous solution pitting attack are critical to the autocatalytic process.

Chloride ions also aid in the formation of local galvanic cells, which can be formed for example by the deposition of copper from solution or by impurities of inhomogeneities at the alloy's surface [Ref. 5].

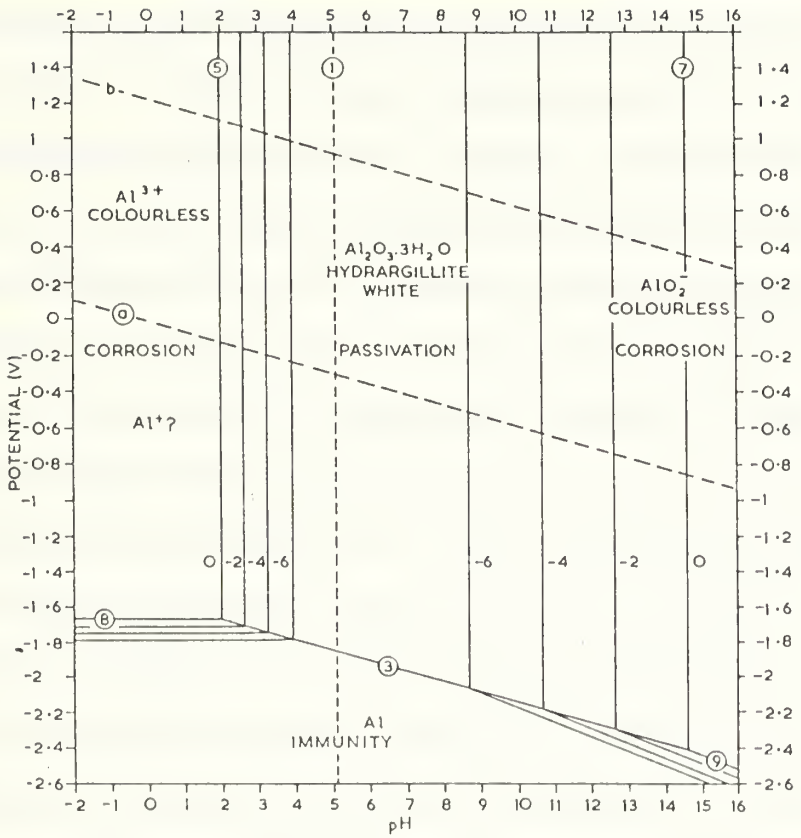

Potential versus pH diagram for Al/H_2O system at 25°C (after *Corrosion*, **14**, 496t (1958))

Figure 1: The Pourbaix diagram for aluminum and its alloys in water. For a nominal corrosion potential of -0.78 V, aluminum is more susceptible to corrosion at pH 4 than at pH 8. This may be due to higher oxide dissolution rates at pH 4.

B. CORROSION OF METAL MATRIX COMPOSITES

P. P. Trzaskoma [Ref. 7] summarizes the probable mechanisms of the corrosion of MMCs as three adverse processes: galvanic coupling of the metal and reinforcement; crevice attack at the metal/reinforcement interface; and preferred localized attack at structural and compositional inhomogeneities within the metal matrix.

The major drawback to MMCs lies in the chemical incompatibility of the metallic matrix with the reinforcement material. Wetting agents applied to fibers are necessary for the matrix metal to infiltrate fiber bundles during composite formation. The high formation temperatures necessary often cause an oxide interface to form between matrix and reinforcement. Radically different thermal expansion coefficients between matrix and reinforcement can lead to a high matrix dislocation density and large thermal residual stresses upon cooling. In addition, differing electrochemical properties of the matrix and reinforcement can lead to unusual and accelerated corrosion.

Some of the classical corrosion tests used on monolithic matrix metals must be modified when applied to MMCs. Coupon weight loss over a period of time, for example, is not an appropriate measure of corrosion rate for aluminum–graphite composites since these materials show an initial weight *gain* as aluminum oxide is formed and trapped within the composite [Ref. 8]. Exposure or non–exposure of the fiber–matrix interface to the corrosive medium must be

considered. Any mechanical, chemical, or corrosion damage sufficient to penetrate the surface foil must also be accounted for.

M. G. Vassilaros et. al. [Ref. 8] found that seawater pitting perforates the surface foils of VSB-32 graphite fiber 6061 aluminum MMCs after twelve weeks immersion, allowing seawater to come into contact with the aluminum-graphite interface. When this occurred, the rapidly accumulating aluminum corrosion product blistered the composite, exposing more of the surface area to corrosive attack. Samples exposed without edge protection demonstrated accelerated corrosion of the metal matrix, which appeared as if it would continue until all of the aluminum was oxidized.

W. H. Pfeifer [Ref. 9] studied the corrosion of Thornel-50 graphite fiber 202 aluminum MMCs in sea water. He found that exfoliation/delamination of the MMCs began preferentially at panel edges parallel to the fiber direction, and rarely at panel edges perpendicular to the fiber direction. Once initiated at the parallel edges, the wedging action of the corrosion products opened up the perpendicular edges. Elimination of interfoils during the consolidation of the composite was found to increase corrosion resistance.

M. Metzger and S. G. Fishman [Ref. 10] found in a review of the literature that in some cases corrosion would proceed into various fiber reinforced MMCs through fiber bundles, in regions of high fiber density. This was attributed to inadequate fiber wetting during

infiltration, since areas of fiber–fiber contact were observed. Well-bonded composites appeared to exhibit good corrosion resistance.

D. M. Aylor and P. J. Moran [Ref. 11] found that the presence of graphite in a graphite fiber 6061 aluminum MMC did not cause an electropositive shift in corrosion potential, as would be expected of normal galvanic corrosion, but rather caused an electronegative shift and a substantial decrease in resistance to passive film breakdown. The poor performance of aluminum–graphite MMCs in marine environments was blamed on this decrease in resistance. The corrosion resistance of the composite was highly dependent upon the integrity of the aluminum surface foils. Corrosion of the surface foils proceeded at a rate typical of monolithic metals until the foil was penetrated, when accelerated corrosion occurred. Partial deaeration was necessary to clearly observe the breakdown and repassivation potentials using cyclic anodic polarization.

A later study by D. M. Aylor and P. J. Moran [Ref. 12] showed that thermomechanical processing of the aluminum foils used for composite fabrication may be responsible for shifting their corrosion potential (E_{corr}) in the electronegative direction, as compared to that of the monolithic alloy. The aluminum foil was prepared by cold rolling and diffusion bonding during the composite fabrication. The E_{corr} of the graphite–foil couple was found electropositive to the foil's E_{corr}, indicating that the graphite fibers were polarizing the foil in a galvanic manner. Corrosion potentials were measured after thirty day's immersion in ASTM ocean water.

D. M. Aylor and R. M. Kain [Ref. 13] reported the dominant corrosion mechanism for aluminum–graphite composites in marine environments is accelerated galvanic corrosion between the aluminum and the graphite fibers. Variations in the surface foil alloy (1100 versus 5056 versus 6061) did not significantly affect the corrosion resistance of the composite. Galvanic coupling was not found to occur in aluminum MMCs reinforced with continuous silicon carbide fibers, even when no edge protection was employed during immersion tests.

A. J. Sedriks et. al. [Ref. 14] studied the effects of galvanic coupling on the corrosion behavior of an aluminum–boron composite in a NaCl solution. They found galvanic coupling not to be a problem, and attributed it to the low electrical conductivity of boron, even though localized corrosion at the interface was observed.

S. L. Pohlman [Ref. 15] found no galvanic interaction between virgin boron fibers and aluminum. When the fibers were extracted from an aluminum–boron MMC, however, they did galvanically couple with the aluminum. His results indicated that the galvanic corrosion occurred between the aluminum matrix and the aluminum boride intermetallic formed during fabrication at the matrix/filament interface. The matrix was anodically attacked, and the intermetallic cathodically protected.

While a literature search uncovered no published work indicating an electrochemical role of aluminum carbide in corrosion, it is expected to play an important mechanical role. B. Maruyama and L. Rabenberg [Ref. 16] proposed that phosphorus and boron compounds

may be effective inhibitors for aluminum carbide formation at the aluminum-graphite interface. Chemical deposition of the compounds on the graphite surface prior to composite consolidation may delay the onset of carbide formation. Alloying the aluminum with borides or phosphides would provide an effectively infinite source of boron or phosphorus to the interface, and perhaps delay the formation of aluminum carbide indefinitely.

C. RESEARCH OBJECTIVES AND OVERVIEW

The purpose of this research was to characterize the corrosion behavior of a P-130x graphite fiber reinforced 6063 aluminum metal matrix composite in aqueous 3.5% sodium chloride. Both electrochemical and immersion techniques were utilized. The effects of varying solution pH, the presence of sulfite ions, and various heat treatments were investigated. A monolithic 6063 aluminum alloy was used as a control, and its corrosion behavior compared to that of the MMC.

A summary of corrosion and electrochemical theory and analytical expressions is presented prior to discussing procedures and results.

II. CORROSION THEORY AND EXPERIMENTAL ELECTROCHEMICAL TECHNIQUES

The long-term nature of corrosion processes makes a rapid laboratory evaluation and prediction of corrosion behavior difficult. Ideally, a quick and easy lab test could be correlated with actual corrosion behavior to develop a convenient gauge of how a second material would corrode. In actuality, no one test can make that prediction, but a well thought-out series of experiments can be very informative and predictive.

The electrochemical nature of corrosion can be used to explain many corrosion processes. Conversely, electrochemical measurements of corrosion in a controlled environment can provide information concerning corrosion rates and susceptibilities. Careful manipulation of only one variable in the corrosion equation at a time may be used to determine the role it plays.

A. CORROSION POTENTIAL

A metal, immersed in a conductive electrolyte, will experience both cathodic and anodic reactions upon its surface. In the absence of galvanic coupling or an externally impressed current or voltage, the predominant cathodic and anodic reactions will polarize together. A corrosion potential and current characteristic to the metal/electrolyte

system will be reached, such that there is no net deposition of charge upon the metal.

When aluminum experiences this single-metal corrosion in aqueous solution, the anodic reaction is aluminum ion dissolution:

$$Al \rightarrow Al^{+++} + 3e^{-}$$

A typical cathodic reaction in aerated solutions is the reduction of oxygen. In near neutral or basic pH, this reaction is:

$$\frac{1}{2}O_2 + H_2O + 2e^{-} \rightarrow 2OH^{-}$$

In aerated acidic solutions, the predominant oxygen reduction reaction is:

$$\frac{1}{2}O_2 + 2H^{+} + 2e^{-} \rightarrow H_2O$$

In deaerated acidic solutions, the cathodic reaction is the evolution of hydrogen:

$$2H^{+} + 2e^{-} \rightarrow 2H \rightarrow H_2$$

The corrosion potential is measured relative to a reference electrode, often a saturated calomel electrode. Tabulated and compared, the corrosion potentials may be used to determine which electrode of a galvanic couple will be the anode and which the cathode, and to predict what voltage will be developed across the cell. In addition, the variation of the corrosion potential with time can yield information about passive layer breakdown or formation.

B. TAFEL EXTRAPOLATION

The corrosion potential is measured in a passive manner, i.e., with no external driving force applied to the working electrode. While the corrosion potential is a useful parameter, it does not quantify the kinetics of the corrosion process. Hence the corrosion current, measured via a technique known as Tafel extrapolation, is often used to make predictions of the corrosion rate of the material. As the corrosion current occurs between microscopically close anodic and cathodic portions of the working electrode, it cannot be measured directly, but must be inferred.

In the Tafel extrapolation technique, the working electrode is driven cathodically to a set potential, and then the potential is swept anodically past the corrosion potential. As the voltage is swept, both it and the current flowing in the system are measured. When the voltage is plotted against the log of the current density, a linear region on both the anodic and cathodic legs near the corrosion potential is often observed. The slopes of the linear regions, usually measured in mV/decade of current density, are known as Tafel constants. The single metal corrosion current density (i_{corr}) is then obtained by extrapolating these linear regions till they intersect. Finally, the corrosion rate, which is proportional to i_{corr}, can be determined using Faraday's law, as shown in Appendix A.

The Tafel extrapolation provides an extremely rapid means of determining the corrosion rate when compared with weight-loss

results, and is even more important considering that weight loss results are not meaningful for determining a penetration rate for composites. Besides i_{corr}, values of E_{corr} and the Tafel constants can also be obtained using the Tafel extrapolation technique. In order to ensure reasonable accuracy, the Tafel region must extend over a current range of at least one order of magnitude. This is not achievable in many systems due to interference from concentration polarization. In addition, it can be applied only to systems containing one reduction process, since the Tafel region is usually distorted if more than one reduction process occurs. A more accurate evaluation of the corrosion current may be made by determining the Tafel constants from independent anodic and cathodic legs, and then performing a polarization resistance measurement.
[Ref. 17:pp. VII 13-28]

C. POLARIZATION RESISTANCE

The electrochemical technique of Polarization Resistance (sometimes referred to as Linear Polarization) is another method of measuring corrosion rates. The technique is performed by applying a controlled-potential scan over a small range, typically 25mV on either side of the corrosion potential. The resulting current is linearly plotted versus potential. The slope of this potential-current function at E_{corr} is referred to as the Polarization Resistance (R_p), and is used in conjunction with the Tafel constants obtained from the Tafel plot to

determine i_{corr}. The procedure for determining i_{corr} from polarization resistance plots is detailed in Appendix B. [Ref. 17:pp. VII 29-37]

The polarization resistance method has several advantages over Tafel extrapolation. The potential does not range as far from E_{corr}, so the surface of the specimen is not significantly affected. It is often quicker than Tafel extrapolation, as the range over which the potential is scanned is less. Tafel constants typically do not vary over a wide range, and frequently one can use an estimated value of 0.1 V/decade for each constant. In the worst case, the calculated corrosion rate would be within a factor of 2.3 of the value which would have been obtained using the actual values of the Tafel constants. In this research, the Tafel constants were determined from a Tafel plot, and then used for the various polarization resistance measurements. [Ref. 17:pp. VII 29-37]

D. CYCLIC ANODIC POLARIZATION

While no cyclic anodic polarization measurements were performed for this thesis, an understanding of cyclic anodic polarization and its two characteristic potentials, the breakdown and repassivation potentials, is necessary for an understanding of the electrochemical measurement of pitting susceptibility.

Cyclic polarization is applicable to any alloy system which utilizes a passive oxide film to protect it from the environment. Rather than focusing on what occurs in the vicinity of E_{corr}, cyclic polarization

studies the behavior of the alloy in the vicinity of the anodic current "knee", which is the region of an anodic scan where the current increases dramatically with applied potential. In cyclic polarization, an anodic scan is started at some pre-determined level, usually E_{corr}, and is moved upward in potential to some point beyond the "knee". The scan is then reversed, and is moved cathodically to a pre-determined final potential.

Two characteristic potentials are extracted from the resultant curve. The first is the breakdown potential (E_{bd}), that potential where the "knee", or rapid current increase is seen in the anodic scan. On an alloy system generally susceptible to pitting and crevice corrosion attack, a hysterisis loop is observed on the cathodic leg of the scan. The potential at which the reverse scan intersects the forward scan is known as the repassivation potential (E_{rp}). [Ref. 17:pp. VII 56-60]

Controversy exists in the literature as to the physical interpretation of these characteristic potentials. Historically, both potentials were believed to be characteristic solely of the alloy system and electrolyte. E_{bd} was thought to be that potential above which the oxide layer could spontaneously decompose locally, and initiate pitting. E_{rp} was thought to be that potential below which those same pits would spontaneously repassivate by forming an oxide layer, and pitting would cease. Where E_{corr} fell compared to these two potentials would predict the behavior of the alloy/electrolyte system. Above E_{bd}, the alloy would spontaneously pit. Below E_{rp}, the alloy would not pit,

and any pits present would not propagate. Between E_{bd} and E_{rp}, no new pitting would initiate, but existing pits would continue to grow. [Ref. 18]

More recent work indicates that the only true characteristic potential for aluminum alloys is E_{rp}, and that E_{bd} is an artifact of the experimental set-up. E_{bd} has been found to be influenced by incubation time (the time the sample was immersed in the electrolyte prior to the test commencing) and the exposure temperature [Ref. 3]. The physical interpretation was that a thicker, more protective film would require a longer induction time for breakdown [Ref. 3]. E_{bd} also varies considerably with the gas used to aspirate the electrolyte prior to and during the cyclic polarization measurement [Ref. 19], and with different fabrication methods used in the preparation of the experimental material [Ref. 12]. Since E_{bd} is a function of the experimental set-up, it is of limited use for general predictions. The repassivation potential has been found to correlate with pitting susceptibility. If E_{corr} is active to E_{rp}, the material is immune to pitting, and if it is noble to E_{rp}, the material is susceptible to pitting. R. A. Bonewitz [Ref. 3] found that the breakdown potential is a function of the ability of the chloride ion to penetrate the oxide film. He inferred that the repassivation potential is the potential at which competitive adsorption favors an oxygen atom over the chloride ion under bulk concentration conditions. D. M. Aylor and P. J. Moran [Ref. 20] found that with sufficient incubation time in a chloride ion containing electrolyte, pit initiation and propagation will occur in

aluminum alloys at potentials at or slightly above the repassivation potential. They found the repassivation potential to be the only characteristic potential for aluminum.

While the meaningfulness of E_{bd} is debatable for aluminum alloys, B. E. Wilde found that the magnitude of (E_{bd} - E_{rp}) and the size of the hysterisis loop related to the crevice corrosion weight loss in stainless steels [Ref. 18]. This is while he has demonstrated E_{bd} to be a function of experimental technique, in particular the amount of pit propagation allowed to occur prior to repassivation.

E. CYCLIC GALVANOSTAIRCASE POLARIZATION

Because of the method-induced variations in E_{bd} (and to a lesser extent, E_{rp}) when using cyclic polarization, S. T. Hirozawa [Ref. 21] developed a technique called galvanostaircase polarization. Instead of controlling the potential, as in cyclic anodic polarization, in galvanostaircase polarization the current is controlled. Hirozawa blames the variability of E_{bd} on the "passivity" of a potential controlled polarization technique. With potential controlled breakdown, the voltage is raised across the passive layer until the charge breaks through the passive layer. In current controlled breakdown, the breakdown is programmed into the experiment, and there are no induction effects.

As the name suggests, in galvanostaircase polarization a stepped sequence of current levels is applied to the sample. The voltage transients of the sample are recorded. The staircase starts at zero

current, steps up to a maximum through a series of regular steps, and then steps down to zero current using the same series of regular steps. The steady-state potentials at the end of the up-steps is extrapolated to zero current to obtain E_{bd}, and the steady-state potentials at the end of the down-steps is extrapolated to zero current to obtain E_{rp}. Schematic current and voltage plots are shown in Figure 2.

The American Society for the Testing of Materials (ASTM) recommends conducting cyclic potentiodynamic polarization measurements for determination of localized corrosion susceptibility (pitting and crevice corrosion) of iron-, nickel-, or cobalt-based alloys [Ref. 22], and cyclic galvanostaircase polarization measurements for determination of localized corrosion susceptibility (pitting and crevice corrosion) of aluminum alloys [Ref. 23].

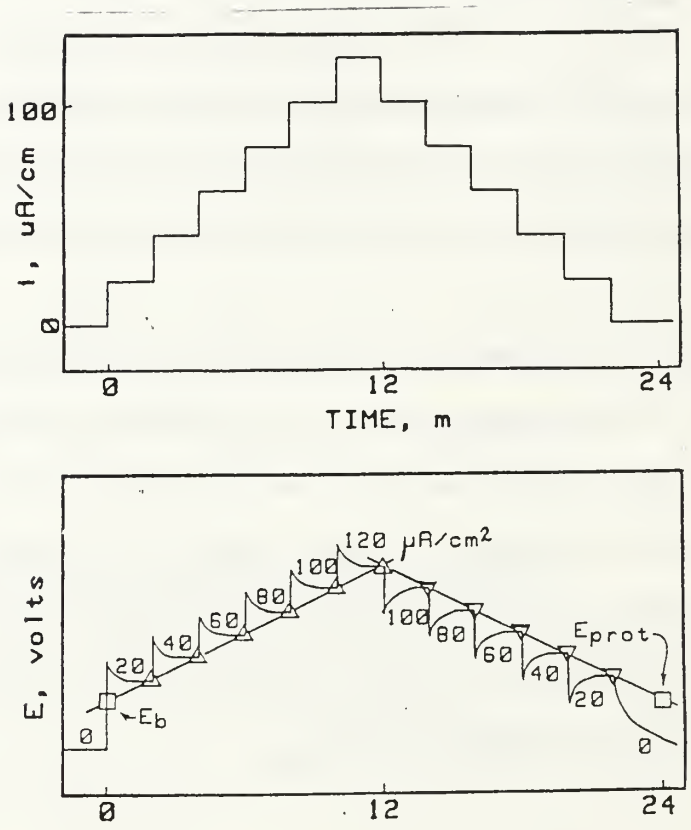

Figure 2: Cyclic Galvanostaircase Polarization. The stepped sequence of electrical current is applied to the sample, and the voltage transients are measured. Extrapolation of the steady-state potentials to zero current yields the breakdown potential.

F. GALVANIC CORROSION

Electrochemical measurement of galvanic corrosion involves passive measurement of the current between dissimilar electrodes in the same electrolyte, or the potential of the corroding couple versus a standard reference electrode. The more active electrode in the couple will act as the anode, while the more noble will act as the cathode. In galvanic corrosion current measurements, the electrodes are short-circuited, and the current flow between them measured. The potential of the shorted couple is measured simultaneously. [Ref. 17:pp. VII 55-56]

As two working electrodes are required, vice the one for all other electrochemical methods discussed previously, a different electrical set-up of the corrosion apparatus is used. This will be covered in greater detail in the procedures section.

III. EXPERIMENTAL EQUIPMENT AND PROCEDURES

A. MATERIALS

The P-130x graphite fibers used both in the fabrication of the composite and as galvanic corrosion electrodes in this research were obtained from Amoco Performance Products, Richfield, Connecticut. The P-130x is an experimental graphite fiber, as the 'x' designates. The fibers are 10 μm in diameter, and are continuous throughout the length of the composite. While their cross-section is nominally circular, difficulty in fabrication often results in a more irregular cross-section. The fibers obtained directly from Amoco came in a spool-wound two-thousand fiber tow, with no twist.

The control monolithic 6063 aluminum used in this research was obtained from ALCOA as extruded angle stock in the T1 (overaged) temper.

The composite was fabricated by DWA Composites, Chatsworth, California. Fabrication was by a proprietary method which involved laying the P-130x fibers in alternating 0° and 90° biases between layers of 6063 aluminum foils and hot-pressing, yielding a 0-90 cross-plied continuous fiber composite. This "sandwich" was then sintered to form the final composite. The outer surface on both sides of the composite plate is a foil. The finished product was supplied in sheets 0.15 m wide, 0.15 m long, and 0.0015 m thick.

B. SAMPLE PREPARATION

1. Composite and 6063 Monolithic Aluminum

Specimens for most of the electrochemical tests were cut into disks 0.015 m in diameter. The material was first cut into manageable pieces. For the monolithic 6063 aluminum, this was accomplished on a power hacksaw. The composite was sandwiched between two pieces of aluminum and then fed through a fine-toothed power bandsaw. Both the monolith and composite disks were cut in their final stages through electric discharge machining using a brass electrode. The monolithic metal electrodes for the galvanic corrosion runs were machined to a 0.0151 m by 0.020 m by 0.003 m rectangular slab, and then tapped to accept the specimen holder rod on one of the 0.0151 m by 0.003 m faces. Immersion tests were conducted on coupons of composite material measuring 0.014 meters long by 0.007 meters wide by 0.0015 meters thick.

Immediately prior to all experiments, the metal and composite specimens were wet sanded to 600 grit on SiC paper. With the composite this was done most carefully, to avoid perforation of the surface foil. The specimens were then washed with tap water, distilled water, and ethanol, and dried under a hot air gun. They were then immersed in boiling acetone for sixty seconds to remove any organic contaminants from the surface.

2. Graphite Fiber Electrodes

Graphite Fiber Electrodes were utilized as the second working electrode in the galvanic corrosion experiments. They were constructed by soldering a short length of fiber tow, usually 0.05 m, to a copper wire. The wire was then threaded through a 0.10 m length of glass tubing, until a 0.015 m length of fiber was also within the tube. That end of the tube was then carefully plugged with a slow-curing organic epoxy. The free end of the wire, which protruded from the still open end of the tube, was epoxied in place so that no tension was placed on the soldered junction. The free end of the wire and the open end of the tube were then fed into the hole at the center of a rubber stopper to form the final electrode assembly. A schematic drawing of the graphite electrode assembly sans rubber stopper is shown in Figure 3.

The free ends of the graphite fibers were trimmed to present the desired surface area to the electrolyte.

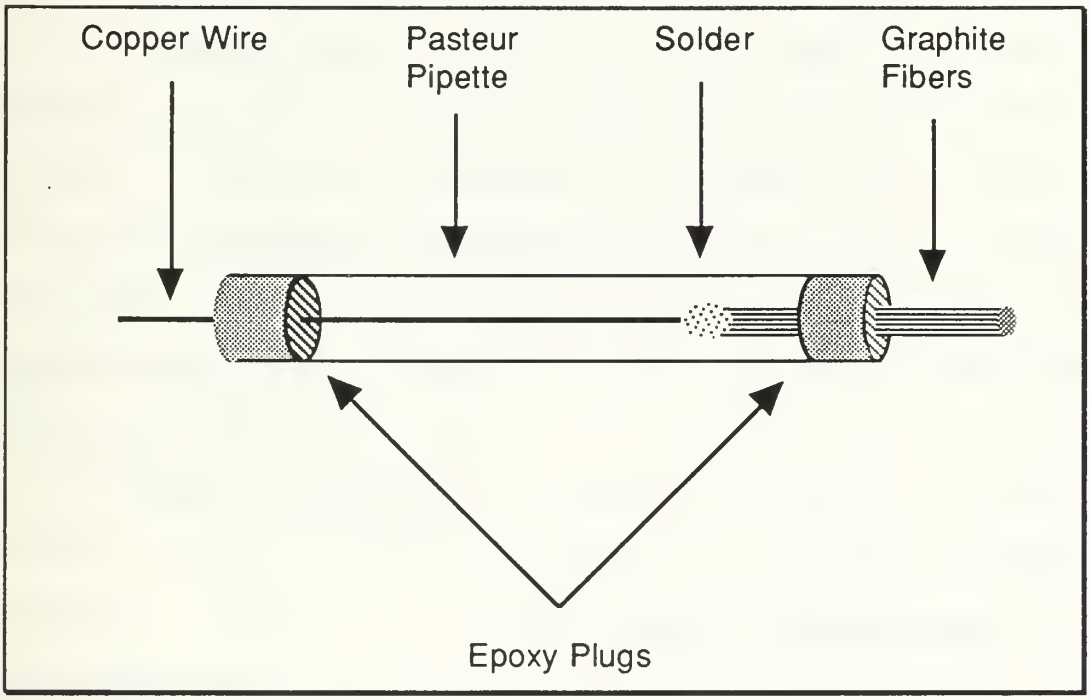

Figure 3: Schematic drawing of the graphite electrode assembly used in the galvanic current measurements. The free ends of the graphite fibers were trimmed to present the desired surface area to the electrolyte.

C. DATA ACQUISITION EQUIPMENT

All electrochemical tests were performed using an EG & G Princeton Applied Research (PAR) corrosion measurement system. The electrodes, aspirator, and electrolyte were contained in a PAR Model K47 Corrosion Cell System. Electrical connections from the cell ran to a PAR Model 273 Potentiostat/Galvanostat. While it is possible to run electrochemical measurements directly from the Model 273, a more powerful approach is to control the Model 273 with a PAR Model 351 Corrosion Measurement System through a parallel interface. The Model 351 used in this research displays the experimental results on the screen, and yields hard copies on a PAR RE0093 Pen Plotter.

1. PAR Model K47 Corrosion Cell

The PAR Model K47 Corrosion Cell consists of a flat-bottomed one liter flask, with five ground-glass fit apertures. The ground-glass nature of the apertures and the adaptors fitted to them allows hermetic sealing of the corrosion environment. Aspiration is accomplished through a purge and vent tube, which are concentric to one another. The purge tube feeds through the center of the aspiration apparatus, bubbling through a large glass frit immersed in the electrolyte. Excess gas rises through the vent tube surrounding the purge tube, and is removed from the corrosion cell. [Ref. 24]

Two high-density graphite counter electrodes and their adaptors occupy two more of the flask's apertures. The graphite

electrodes are necessary when the working electrode is being actively driven by either an impressed current or voltage. [Ref. 24]

The angled aperture accepts the reference electrode assembly, which is held in place by a clamp. The reference electrode is a two-piece assembly, comprised of a bridge tube ending in an unfired frit, and the actual reference electrode. The bridge tube is filled with an electrolyte, which need not be the same as that in the flask, but must not be radically different (e.g. organic solvent in one, aqueous solution in the other). The frit on the end of the bridge tube provides ultra-low leakage rates with a minimum IR drop. The K47 cell is depicted in Figure 4. [Ref. 24]

The large center aperture accepts the specimen electrode assembly. A metal rod, threaded at each end, fits through the ground-glass body. A knurled nut is threaded onto the top of the rod, while a compression gasket is slipped over the bottom of the rod and either the specimen or a K105 flat specimen holder is threaded to the bottom. The knurled knob is tightened, sealing the compression gasket both against the bottom of the glass tube, and the top of the specimen or specimen holder. When the specimen holder is not used, the specimen is usually in the shape of a cylinder tapped along the center axis. When the specimen holder is used, the specimen is in the shape of a disk approximately 0.016 m in diameter. A sealing washer composed of Kalrez, a fluorocarbon elastomer, exposes 0.0001 m^2 of the specimen area to the test solution. [Ref. 24]

For all except the galvanic corrosion runs, the electrical hookup of the corrosion cell to the rest of the data acquisition equipment is identical. Since galvanic corrosion requires two working electrodes, however, its electrical hookup differs slightly, and is detailed in Reference 17.

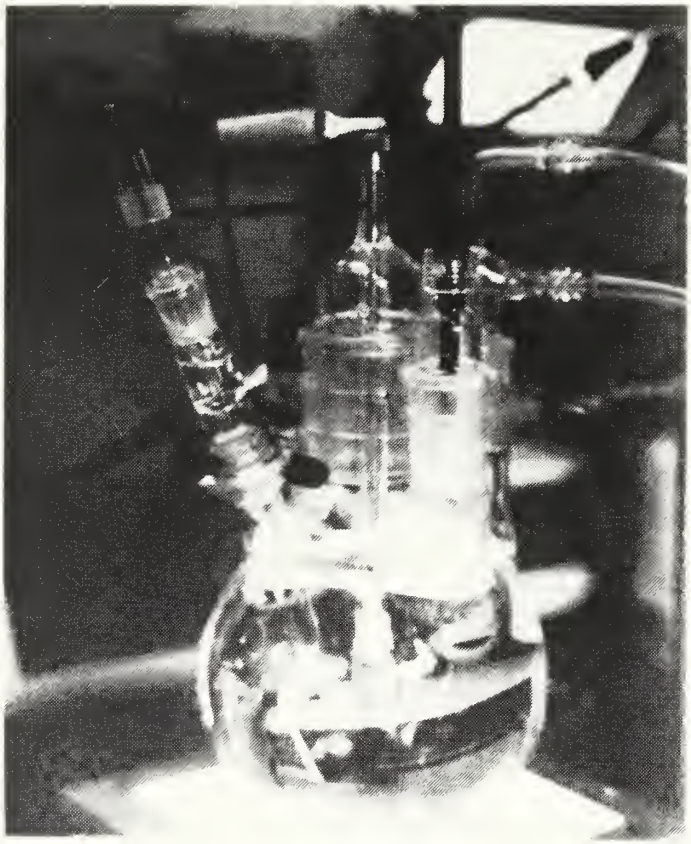

Figure 4: The K47 Corrosion Cell.

2. PAR Model 273 Potentiostat / Galvanostat

The PAR Model 273 Potentiostat/Galvanostat, either by itself, interfaced with a third-party computer, or controlled by the Model 351 Corrosion Measurement System through a proprietary parallel interface, performs the actual electrochemical measurements of and applies any external current or potential required to the K47 corrosion cell. When used by itself, data may be taken from the liquid-crystal display on the apparatus's front. While a greater ease of use and display/output of data is available when controlling the Model 273 with a Model 351, one advantage of operating the Model 273 in a stand-alone mode is that an electrochemical test may be customized beyond the constraints imposed by the Model 351's programming.

3. PAR Model 351 Corrosion Measurement System

The Model 351 Corrosion Measurement System has a user-friendly interface, receiving commands from the user who touches "buttons" on the "touch-screen" cathode ray tube. The Model 351 can simultaneously control up to eight Model 273's, allowing a researcher tremendous flexibility in experimentation. In this research the Model 351 controlled a single Model 273. The experimental electrochemical measurements being carried out by each Model 273/K47 set-up is completely controlled by the Model 351. After the initial set-up, the only switch which must be operated on the Model 273 is the cell enable switch, which physically disconnects the

electrical connection between the Model 273 and the K47 corrosion cell. [Ref. 17:p. I-1]

a. Safety Considerations

During some electrochemical experiments, the Model 273 can develop potentially *fatal* voltages and currents. While the Model 351 has a software switch which disables the power supply to the K47 corrosion cell, this software disconnect should not be solely relied upon. The Model 273 has a Cell Enable switch, which physically disconnects the electrical connection to the K47 corrosion cell. The cell enable switch should be used *whenever* the operator is working on the corrosion cell. [Ref 17:pp. I 1-2]

D. ELECTROCHEMICAL TECHNIQUE PARAMETERS

Twelve general electrochemical techniques are available for individual customization in the Model 351's software. They are: [Ref. 17:p. II-2]

- Direct Cell Control
- Potentiodynamic
- Tafel Plot
- Polarization Resistance (Linear Polarization)
- Cyclic Polarization
- Potentiostatic
- Potentiokinetic Reactivation
- Corrosion Potential
- Corrosion Behavior Diagram
- Galvanic Corrosion

- Galvanodynamic
- Galvanostatic

In this research, Tafel extrapolation, polarization resistance, corrosion potential, galvanic corrosion, and galvanodyamic techniques were used. The galvanodynamic technique was modified to perform galvanostaircase polarization. Each technique may be customized by user-configurable parameters, such as run-time, current step, vertex potential, etc. While each technique comes with default parameters, they were often found to be insufficient for this research. For example, the default settings for cyclic polarization polarizes an aluminum specimen anodically so far as to develop corrosion currents as high as 10,000 ampere per meter squared, a rate which corrodes through 0.003 m of aluminum in a few hours! Default parameters in other techniques caused instability in data acquisition, often when a voltage step was large enough to induce large amounts of transient gas evolution of the specimen. Ascertaining which combination of parameters gives the best results for a particular technique can be tricky, because of the interactive nature of the parameters. For example, a given run can have no more than two thousand data points. This must be borne in mind when determining optimum settings for run-length and data sampling rate.

The parameters settled upon for the techniques used in this research follow. The details of performing the electrochemical tests are described in Reference 17. For all experiments except galvanic corrosion measurements, the specimen was a disk contained in the

K105 flat specimen holder, with 0.0001 m^2 of surface area exposed to the electrolyte.

1. Corrosion Potential Test Parameters

As the measurement of corrosion potential is an entirely passive examination of the working electrode / electrolyte system, the only parameter which must be specified is time. Run lengths were initially forty–eight hours, but were shortened to twenty–four hours once it was determined that by that point the corrosion potential has essentially stabilized.

A number of curve smoothing choices are available for each test. In all cases, seven point smoothing was employed.

2. Tafel Plot Test Parameters

A number of Tafel plots were performed, but only one was used to provide Tafel constants for the i_{corr} computations in linear polarization. The systems studied did not lend themselves easily to Tafel plots. Tafel plots span over a substantial potential range, and as the system stepped through that voltage range there was instability in data acquisition. The voltage steps were large enough to induce large amounts of transient gas evolution on the specimen during the cathodic leg. Tafel plot test parameters were:

- Initial E : - 50 mV below E_{corr}
- Final E : 50 mV above E_{corr}
- Initial Delay : 600 seconds
- Smooth: Seven Point
- Scan Rate: 0.05 mV/s

- IR Compensation: Disabled
- Area: 1 cm^2

3. Polarization Resistance Test Parameters

The Tafel constants determined from the Tafel plot were input into the polarization resistance measurements to enable the automatic computation of i_{corr}.

- Initial E: - 20 mV below E_{corr}
- Final E: 20 mV above E_{corr}
- Initial Delay: 3600 seconds
- Scan Rate: 0.01 mV/s
- Equivalent Weight: 13.49 g/equiv
- Density: 2.7 g/cm^3
- Area: 1 cm^2
- β Anodic: 0.058 V/decade
- β Cathodic: 0.171 V/decade
- Smooth: Seven Point
- IR Compensation: Disabled

4. Cyclic Galvanostaircase Polarization Test Parameters

In these cyclic galvanostaircase polarization experiments, the current was stepped up to a maximum, and then stepped down back to zero amperes. An initial delay of 120 seconds was used in order for E_{corr} to be readily displayed, but it must be remembered that the length of the initial delay is not important, as oxide breakdown is pre-programmed by the current-control technique.

- Initial I: 0 μA
- Vertex I: 120 μA
- Final I: 0 μA

- Initial Delay: 120 s
- Threshold E: Pass
- Step I: 20 μA
- Smooth: Seven Point
- Step Time: 120 s
- Measurements per Step: 120
- Area: 1 cm^2

5. Galvanic Corrosion Test Parameters

In the galvanic corrosion measurements the metal working electrode was a rectangular slab of monolithic Al 6063, measuring 0.02 m x 0.0151 m x 0.003 m. With 0.000015 m^2 obscured by the Teflon compression gasket, the total surface area of the metal working electrode exposed was 0.0008 m^2. The run time was twenty-four hours, using seven-point smoothing.

The second working electrode was composed of a two-thousand fiber tow of P-130x graphite fibers. By varying the length of the tow, the percentage of total surface area of the combined working electrodes which was graphite could be varied. Area fractions of 0.10 and 0.40 were used in this research. Calculations of the graphite fiber lengths necessary are detailed in Appendix C.

E. IMMERSION TESTING

Immersion testing was performed over a 22 day period in 0.50 liter volumes of unbuffered 3.5% NaCl aqueous solutions. The pH and ionic contents of the solutions for the seven immersion trials are detailed in Table 2. The reagent used to adjust the pH is also shown in

the table. The equivalent of 1.25 ml of sulfurous acid in 900 ml 3.5% aqueous NaCl lowered the pH to 4. This corresponds to a sulfite ion concentration of 82 ppm. This same concentration was used in all tests involving sulfite ions. The tests were performed on 0.014 m by 0.007 m by 0.0015 m coupons of the composite. The upper and lower surface foils exposed only matrix metal to the electrolyte, while the edges exposed both graphite fiber and matrix metal. Because of the cross-plied arrangement of the fibers in the composite, some of the exposed fibers were parallel to the edge, while others were perpendicular to it. The edges of some of the immersion coupons were coated with a thin run of epoxy 48 hours prior to the immersion testing. One edge of each unprotected coupon was polished with 1 μm diamond paste prior to immersion testing, to facilitate microscopic examination.

The prepared coupons were placed onto immersion racks constructed from glass slides. They were lowered into beakers containing the immersion solutions. The solution levels were marked on the side of the beaker, and distilled water added daily as needed to compensate for evaporative losses.

At the end of the immersion testing the samples were removed from the solutions and scrubbed under running water with a rubber stopper to remove corrosion products. They were then rinsed with distilled water, rinsed again with ethanol, and dried under a hot air gun before being photographed under a low power microscope.

TABLE 2

SUMMARY OF IMMERSION TESTS

Test #	Heat Treatment	pH	H_2SO_3	Edge Protection	Reagent
1	A.R.	4	No	Yes	HCl
2	A.R.	4	Yes	Yes	H_2SO_3
3	A.R.	4	Yes	No	H_2SO_3
4	S&Q	8	No	Yes	NaOH
5	S&Q	4	Yes	Yes	H_2SO_3
6	A.R.	8	No	Yes	NaOH
7	A.R.	8	No	No	NaOH

IV. RESULTS AND SUMMARY

A. GALVANIC CORROSION CURRENT RESULTS

The galvanic corrosion current values are tabulated below, in Table 3, and presented graphically in Figure 5. The heat treatments examined were as-received (designated as 'A.R.') and solutionized and quenched (designated as 'S&Q'). The galvanic corrosion current density was measured for both heat treatments, at pH values of 4 and 8, and also for two different exposed graphite area fractions (A_f).

TABLE 3

GALVANIC CORROSION CURRENT DENSITY (i_{gal}) in $\mu A/cm^2$

Heat Treatment	pH	i_{gal} for $A_f = 0.1$	i_{gal} for $A_f = 0.4$
A.R.	4	20	350
S&Q	4	2	250
A.R.	8	<1	85
S&Q	8	<1	40

It is seen from Table 3 and Figure 5 that the corrosion current increases with decreasing electrolyte pH. This can be attributed to a change in the oxygen reduction reaction occurring at the cathode. The cathodic half-cell in aerated acidic aqueous solutions is polarized

to a more electropositive potential than the cathodic half-cell in aerated basic aqueous solutions. Assuming that the Tafel slopes and the exchange current densities for the cathodic reactions in aerated acidic and basic electrolytes are not drastically different, it is conceivable from the above that the corrosion current of the galvanic couple will be greater when the solution is acidic (low pH).

Figure 5 also shows that as the area fraction of graphite exposed to the electrolyte increased, the corrosion current increased. This can be explained simply in terms of an 'area-effect'. Increasing the exposed graphite area increases the area of the cathode, which is known to cause accelerated dissolution of the more active electrode (in this case, the 6063 aluminum matrix).

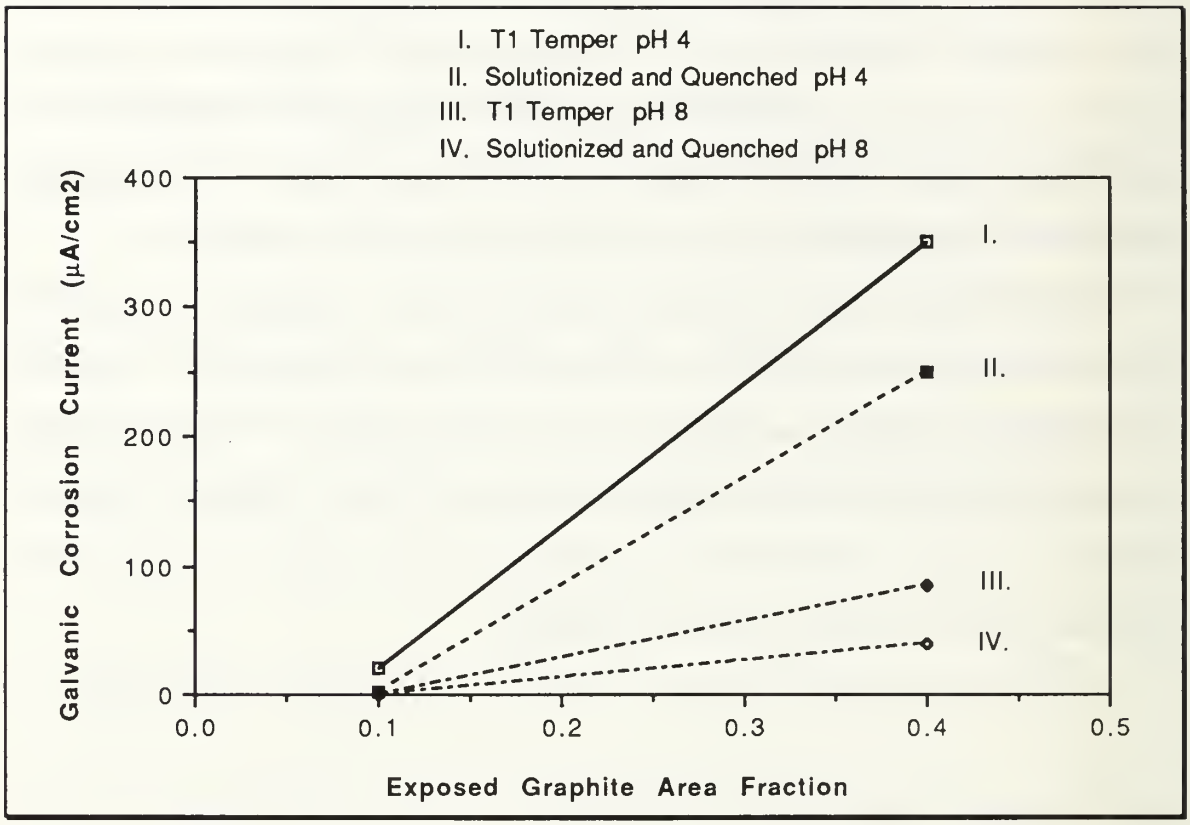

Figure 5 : The galvanic corrosion currents, which are proportional to the galvanic corrosion rates, are shown for a monolithic metal electrode galvanically coupled to a graphite fiber electrode. The current is strongly dependent upon pH and the exposed graphite fraction. Current increases as pH drops or the area fraction increases. Solutionized and quenched samples exhibit lower galvanic corrosion currents than their counterparts in the as received state.

B. PITTING SUSCEPTIBILITY

The corrosion and repassivation potentials for the monolithic 6063 aluminum and the composite are presented in Table 4. The abbreviations used are:

- Al : Monolithic 6063 Aluminum.
- Al–Gr : 6063 Aluminum P–130x Graphite Fiber Metal Matrix Composite.
- A.R. : No heat treatment, in the as–received condition.
- S&Q : Sample was solutionized and quenched.
- S.D. : Composite surface was sanded down to reveal the graphite layers.

Various plots of these data are shown as Figures 6, 7, 8, and 9, to emphasize differences based upon pH and heat treatment. Figures 6 and 7 show a comparison of the corrosion and repassivation potentials of the composite at pH 4 and pH 8. It is seen that in the as–received state, the repassivation potential is very close to or slightly greater than the corrosion potential, making the composite susceptible to pitting at both pH values (Figure 6). The solutionized and quenched composite, however, exhibits a corrosion potential considerable lower than the repassivation potential at pH 8 (Figure 7), thereby making the material resistant to pitting. At pH 4, however, the corrosion potential is electropositive to the repassivation potential. Therefore solutionizing and quenching does not reduce pitting susceptibility at low pH values.

Almost identical trends are seen for the monolithic 6063 aluminum, as shown in Figures 8 and 9. Solutionizing and quenching reduces pitting susceptibility at pH 8, but actually increases it slightly at pH 4.

The decrease in pitting susceptibility at pH 8 on solutionizing and quenching can be explained as follows. At near neutral pH values, the oxide layer on the aluminum is stable, and grows in a thick, hydrated protective layer (Figure 1). At points where the precipitate particles are exposed at the surface, however, the oxide layer is disrupted, and pitting can begin. After solutionizing and quenching, the precipitates dissolve and the oxide layer discontinuities are eliminated, lowering pitting susceptibility. At low pH values, the oxide layer is relatively unstable, encouraging aluminum dissolution regardless of the lack of precipitates.

TABLE 4

CORROSION AND REPASSIVATION POTENTIALS (mV)

Material	Heat Treatment	Buffer or H_2SO_3	pH	E_{corr}	E_{rp}
Al	A.R.	Buffer	4	-774	-780
Al	A.R.	Buffer	8	-784	-791
Al	S&Q	Buffer	4	-750	-769
Al	S&Q	Buffer	8	-774	-742
Al	A.R.	H_2SO_3	4	-782	-823
Al	S&Q	H_2SO_3	4	-775	-763
Al–Gr	A.R.	Buffer	4	-766	-764
Al–Gr	A.R.	Buffer	8	-775	-771
Al–Gr	S&Q	Buffer	4	-751	-768
Al–Gr	S&Q	Buffer	8	-795	-744
Al–Gr	A.R.	H_2SO_3	4	-777	-773
Al–Gr	S&Q	H_2SO_3	4	-780	-766
Al–Gr	A.R. & S.D.	Buffer	4	-805	
Al–Gr	A.R. & S.D.	Buffer	8	-910	
Al–Gr	S&Q & S.D.	Buffer	4	-786	
Al–Gr	S&Q & S.D.	Buffer	8	-920	

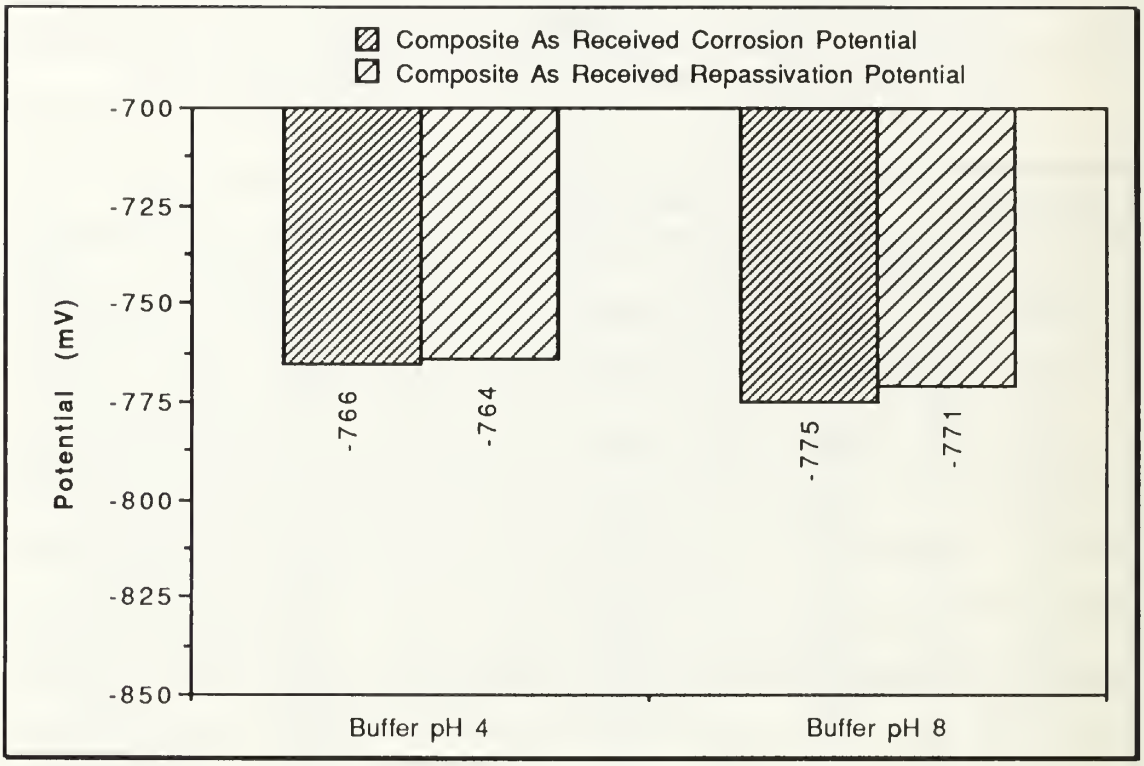

Figure 6: The pitting susceptibility of the composite at pH 4 and 8, in the as received state. A corrosion potential below the repassivation potential indicates immunity to pitting. At both pH 4 and 8, the corrosion and repassivation potentials were insufficiently dissimilar to confer any pitting immunity.

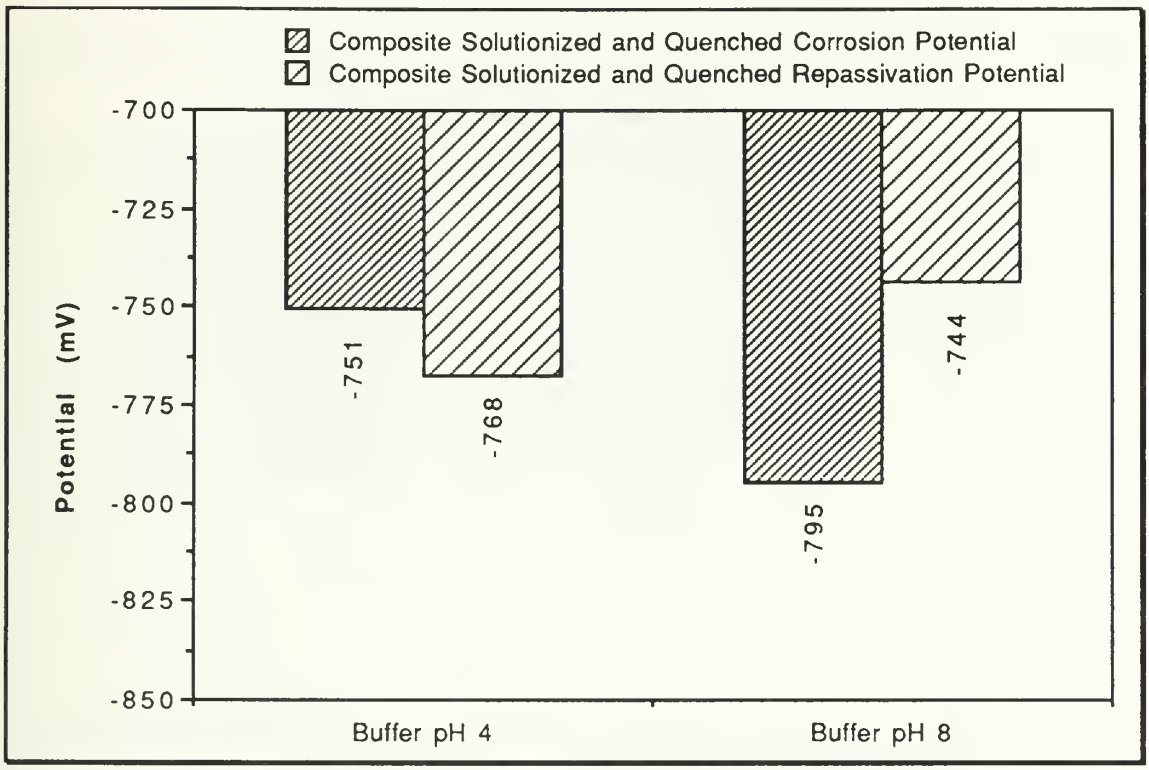

Figure 7: The pitting susceptibility of the composite at pH 4 and 8, in the solutionized and quenched state. A corrosion potential below the repassivation potential indicates immunity to pitting. At pH 4, the heat treatment seems to have increased the susceptibility to pitting somewhat. At pH 8, the heat treatment has conferred immunity to pitting.

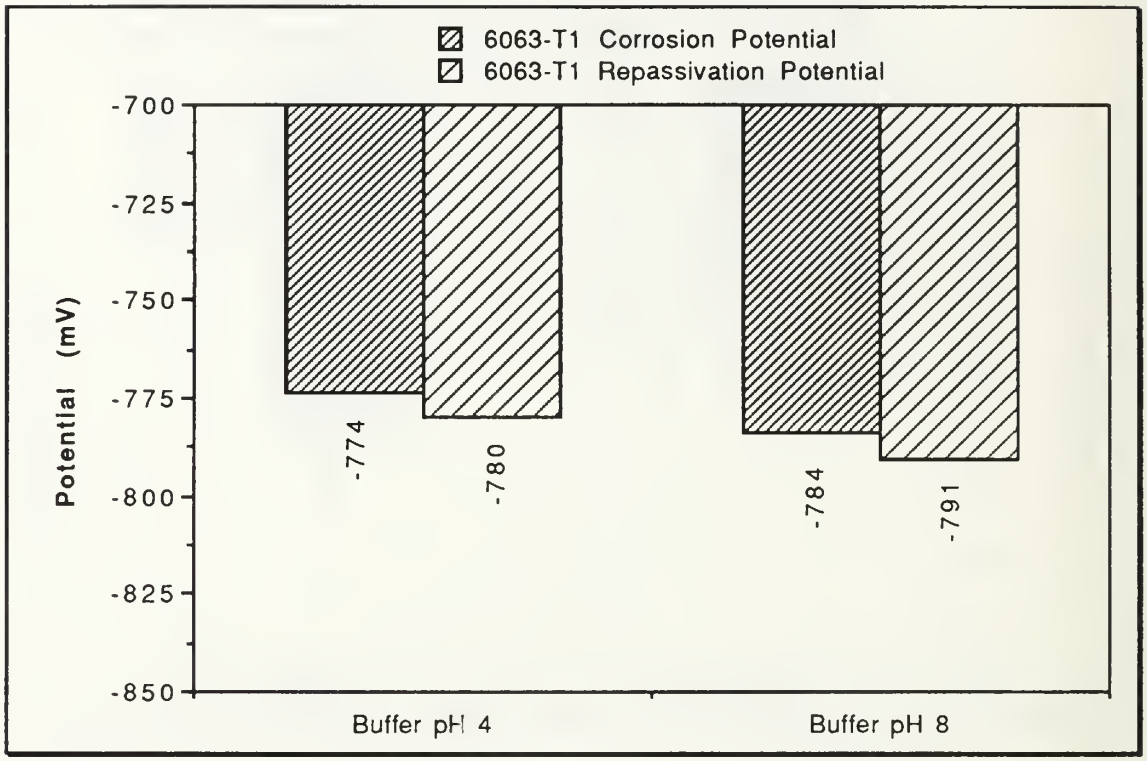

Figure 8: The pitting susceptibility of the monolith at pH 4 and 8, in the T1 temper. A corrosion potential below the repassivation potential indicates immunity to pitting. At both pH 4 and 8, the corrosion and repassivation potentials were insufficiently dissimilar to confer any pitting immunity.

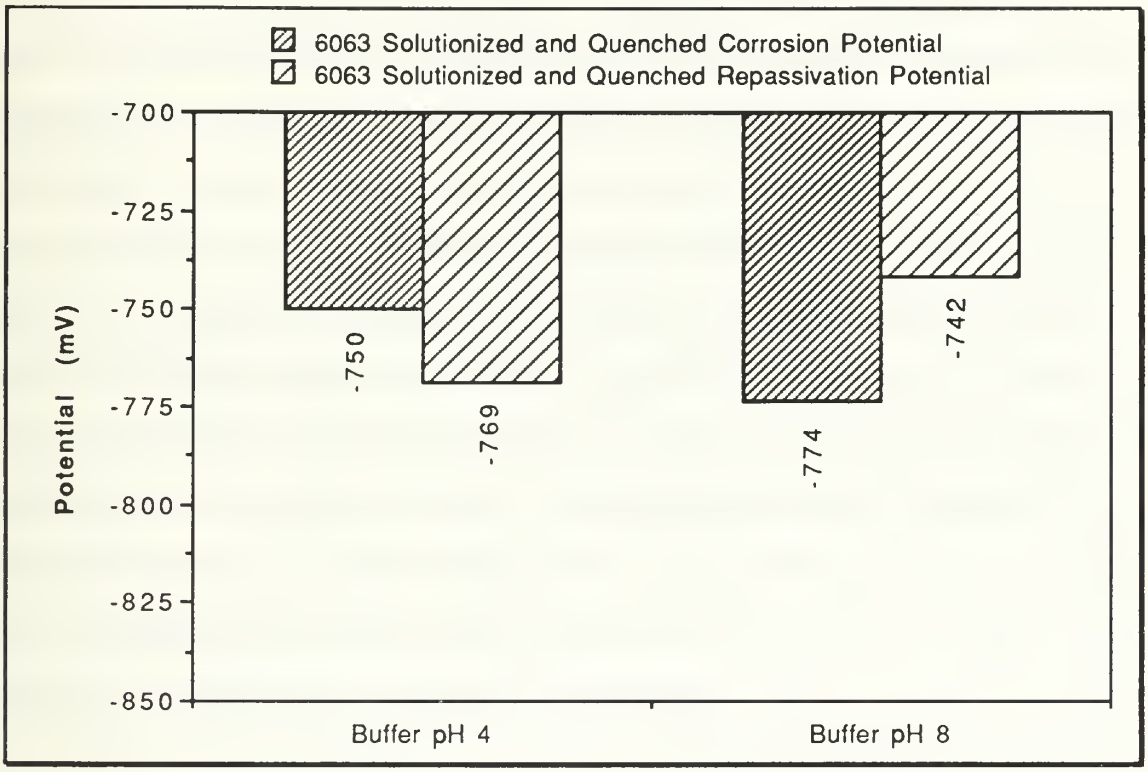

Figure 9: The pitting susceptibility of the monolith at pH 4 and 8, in the solutionized and quenched state. A corrosion potential below the repassivation potential indicates immunity to pitting. As in the composite, the heat treatment seems to have increased the susceptibility to pitting at pH 4. At pH 8, the heat treatment has conferred immunity to pitting.

C. CORROSION CURRENT FROM LINEAR POLARIZATION

The corrosion current (i_{corr}) results from the linear polarization or polarization resistance tests are presented in Tables 5 and 6. Some of the data are reproduced in Figures 10, 11, 12, and 13 to illustrate the effects of pH, heat treatment, and the presence of the sulfite ions. The i_{corr} data for the as-received composite are illustrated in Figure 10, for the solutionized and quenched composite in Figure 11, for the as-received monolith in Figure 12, and for the solutionized and quenched monolith in Figure 13. The Tafel constants were first found by performing a Tafel extrapolation. β_a was determined to be 0.058 V/decade, and β_c to be 0.171 V/decade. The same Tafel constants were used for each computation, and the computations were performed in an iterative manner by the data acquisition equipment. The abbreviations used are:

- Al : Monolithic 6063 Aluminum.
- Al-Gr : 6063 Aluminum P-130x Graphite Fiber Metal Matrix Composite.
- A.R. : No heat treatment, in the as-received condition.
- S&Q : Sample was solutionized and quenched.

In summary, Figures 10, 11, 12, and 13 reveal that the corrosion current is dependent upon pH, and is greater at low pH. This was true both for the composite and the monolith, in either heat treated state, with or without the presence of sulfite ions. This result was expected, on the basis of a changing cathodic half-cell reaction. The four figures also show that i_{corr} is greater for the as-received state

than for the solutionized and quenched state at pH 4. This may be explained by the destabilizing effect that precipitates have upon the protective oxide layer of aluminum. The low values of i_{corr} at pH 8 obscured any effect that heat treating might have on the corrosion current.

Figures 10 and 11 show that the presence of the sulfite ion increases i_{corr} for the composite at pH 4 for both heat treatments. Figure 13 shows that the presence of sulfites ion increases i_{corr} for the solutionized and quenched monolith also. This is attributed to the oxidizing power of SO_3^-. Figure 12 displays anomalous results for the monolith in the T1 temper, as it is the only instance where the sulfite ion appeared to consistently lower i_{corr}. At this point, no explanation can be provided for the anomalous behavior.

Comparison of Figures 12 and 13 to Figures 10 and 11 shows the corrosion current of the monolith was greater than that of the composite's surface foil in nearly all instances. This is tentatively attributed to differing thermomechanical processing history and/or differing actual compositions.

TABLE 5

CORROSION CURRENTS OF MONOLITHIC 6063 ALUMINUM AS DETERMINED FROM LINEAR POLARIZATION

Material	Heat Treatment	Buffer, H_2SO_3, or Both	pH	i_{corr} ($\mu A/cm^2$)
Al	A.R.	Buffer	4	92.7
Al	A.R.	Buffer	8	20.6
Al	A.R.	Both	4	39.2
Al	A.R.	Both	8	4.85
Al	A.R.	H_2SO_3	4	53.9
Al	S&Q	Buffer	4	76.1
Al	S&Q	Buffer	8	8.52
Al	S&Q	Both	4	118.0
Al	S&Q	Both	8	21.0
Al	S&Q	H_2SO_3	4	51.3

TABLE 6

CORROSION CURRENTS OF 6063 ALUMINUM P-130X GRAPHITE FIBER MMC AS DETERMINED FROM LINEAR POLARIZATION

Material	Heat Treatment	Buffer, H_2SO_3, or Both	pH	i_{corr} ($\mu A/cm^2$)
Al-Gr	A.R.	Buffer	4	41.1
Al-Gr	A.R.	Buffer	8	0.497
Al-Gr	A.R.	Both	4	48.1
Al-Gr	A.R.	Both	8	18.1
Al-Gr	A.R.	H_2SO_3	4	33.6
Al-Gr	S&Q	Buffer	4	15.1
Al-Gr	S&Q	Buffer	8	4.39
Al-Gr	S&Q	Both	4	32.0
Al-Gr	S&Q	Both	8	3.09
Al-Gr	S&Q	H_2SO_3	4	69.7

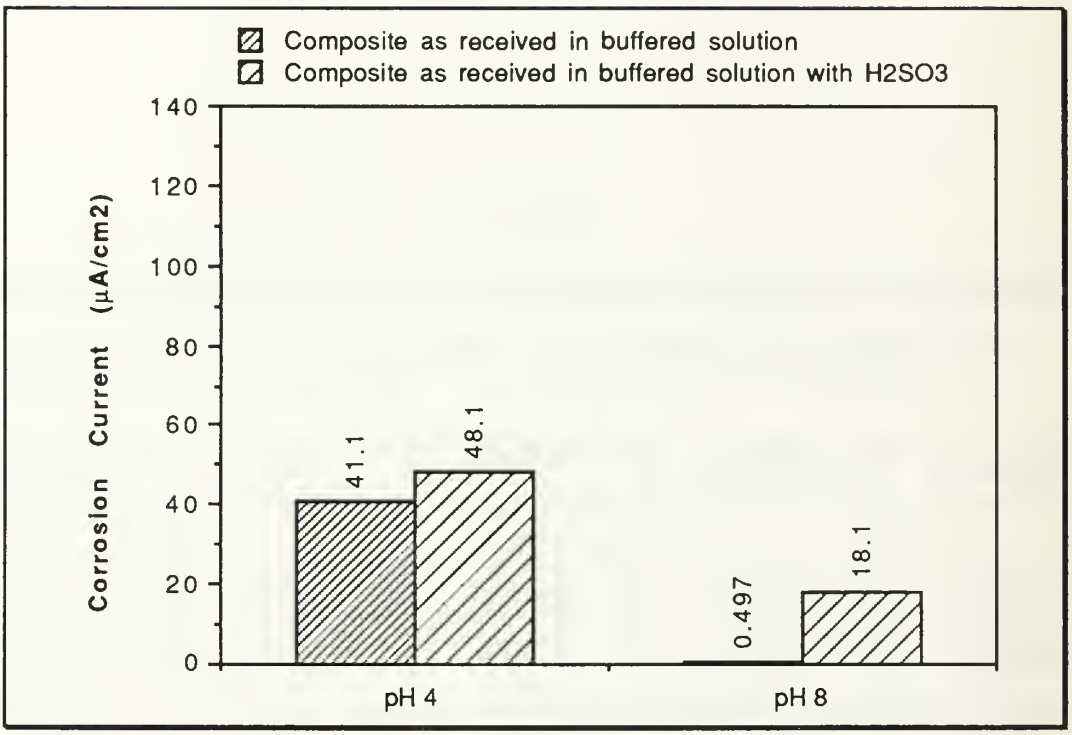

Figure 10: The i_{corr} of the as received composite. The corrosion current was greatest at pH 4. The presence of the sulfite ion increased i_{corr} at pH 4. The effect of the sulfite ion at pH 8 was less certain due to the prevailing low current conditions.

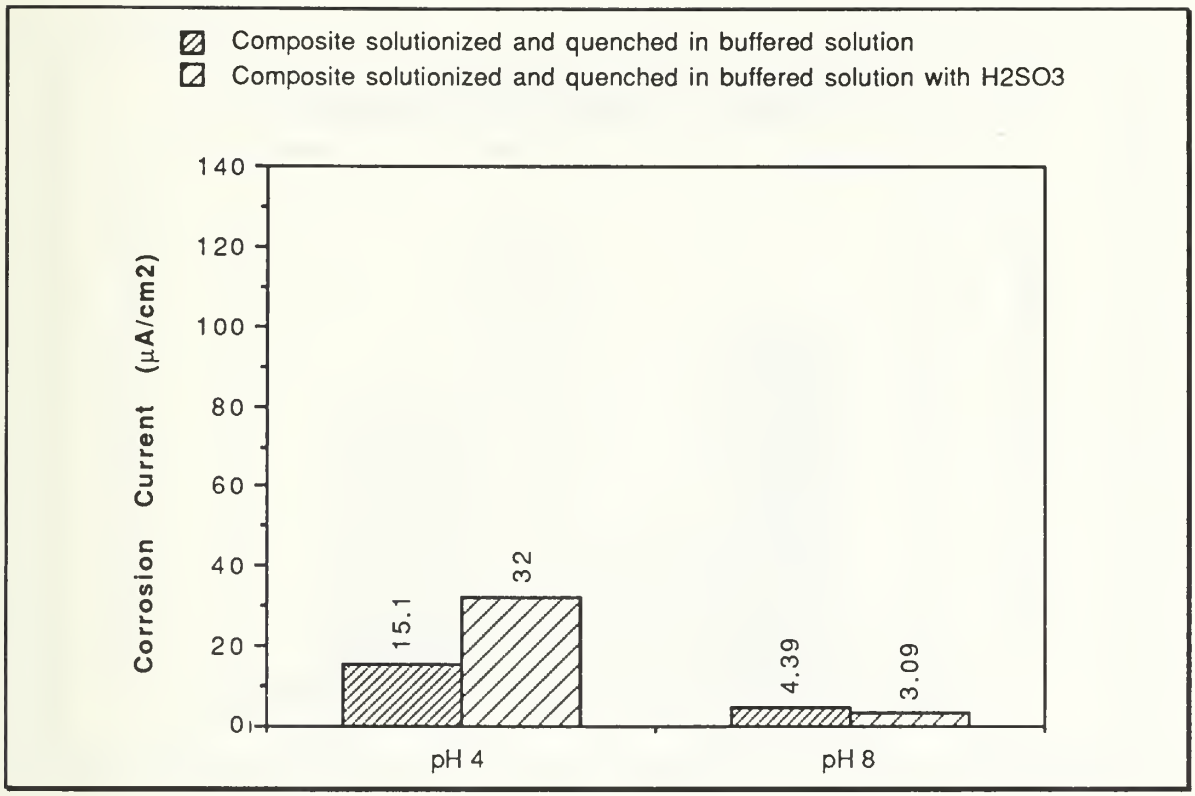

Figure 11: The i_{corr} of the solutionized and quenched composite. The corrosion current was greatest at pH 4. The presence of the sulfite ion increased i_{corr} at pH 4. The effect of the sulfite ion at pH 8 was less certain due to the prevailing low current conditions.

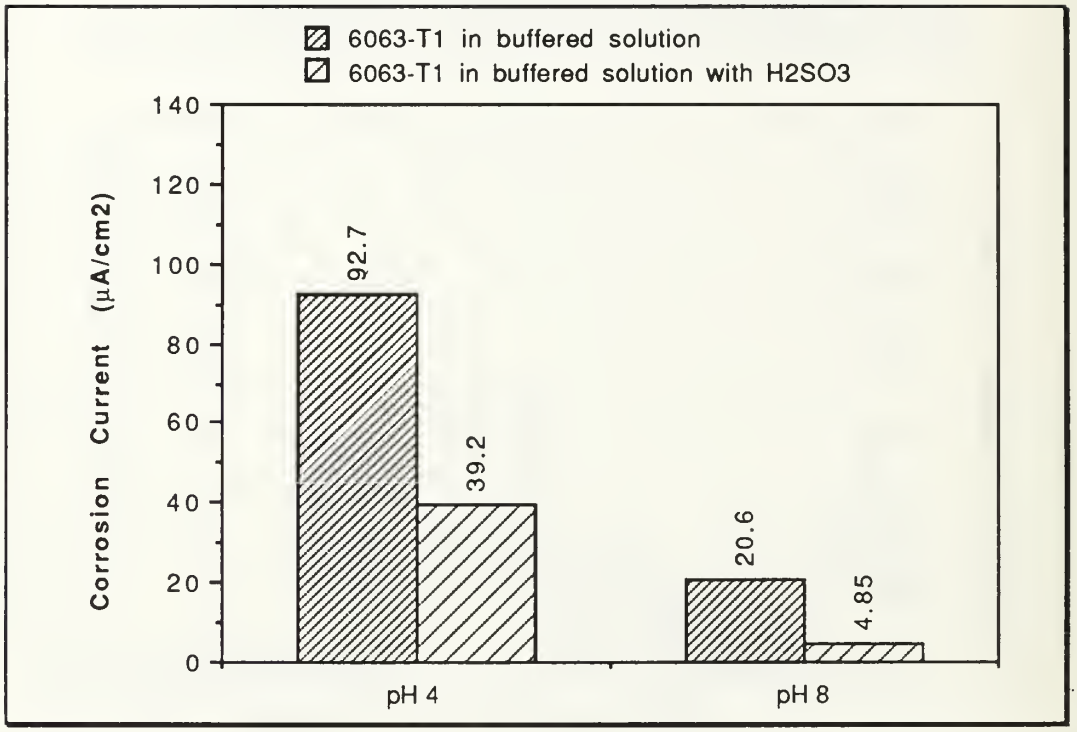

Figure 12: The i_{corr} of the monolithic 6063 aluminum in the T1 temper. The corrosion current was greatest at pH 4. The results were anomalous, as the sulfite ion appeared to decrease the corrosion current in this instance.

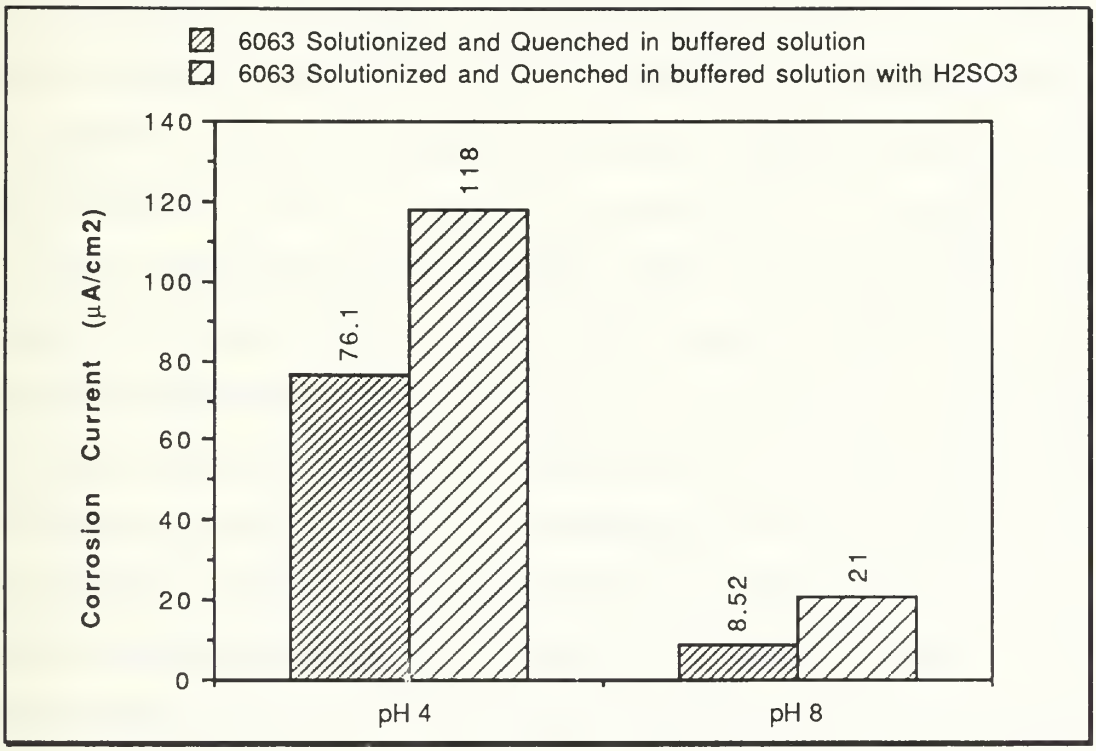

Figure 13: The i_{corr} of the solutionized and quenched monolith. The corrosion current was greatest at pH 4. The presence of the sulfite ion increased i_{corr} at pH 4. The effect of the sulfite ion at pH 8 was less certain due to the prevailing low current conditions.

D. POLARIZATION OF ALUMINUM BY GRAPHITE

Two electrically connected materials of differing corrosion potentials in the same electrolyte form a galvanic cell. If the electrical connection has a very high resistance, the voltage developed by the galvanic cell may be measured. If the corrosion potential of each electrode were measured, they would be found to have not changed. If the resistance of the electrical connection is then lowered to near zero, the galvanic corrosion current flowing through it may be measured. If the corrosion potentials of the electrodes are measured again, they will be found to share a common value midway between their original ones. They are said to have polarized to that value, the anode becoming more electropositive and the cathode electronegative.

During the galvanic corrosion experiments, the galvanic current was of principal interest. The galvanic corrosion potential to which the system polarized was also measured. It would be expected to be electropositive to the corrosion potential of the monolith.

If the surface of the composite is abraded on 600 grit SiC paper to reveal the graphite–aluminum interfaces, they would be expected to galvanically couple. The galvanic current between the graphite fibers and the matrix could not be measured, as the graphite fibers are embedded in the aluminum and an external ammeter cannot be placed between them. The galvanic corrosion potential to which the abraded composite polarizes was measured.

The corrosion potential of the monolith, the galvanic corrosion potential of the 6063 aluminum–graphite couple and the galvanic

corrosion potential of composite abraded to reveal the graphite–aluminum interfaces are presented in Figure 14.

Figure 14 shows that when coupled, graphite polarizes aluminum electropositively, as expected. The corrosion potential of the exposed graphite–aluminum interface of the composite was electronegative to the general corrosion potential of the monolith, which was unexpected.

This unexpected electronegativity may be due to preferential crevice corrosion attack of the interface, or changes in other interfacial corrosion characteristics which are not yet understood. Immersion tests at pH 4 and pH 8 show no visually discernable difference in the corrosion of the composite done to the transverse fiber region. Earlier results (Figure 5) indicate that the rates of galvanic corrosion should have been considerable greater at pH 4. This suggests that a mechanism besides galvanic corrosion, such as crevice corrosion, is in operation. One possibility is that crevice corrosion is stabilizing large anodic areas of aluminum with little or no oxide film. The lack of an oxide film might drive the potential characteristic of aluminum dissolution electronegative, or increase the exchange current density, or both. The net effect of this would be to lower the corrosion potential of the galvanic couple.

Yet another possibility is that galvanic coupling is very local on the surface of the abraded composite, such that the graphite fiber area ratio approaches one. The subsequent shift in exchange current

densities caused by the area affect could conceivably be significantly electronegative.

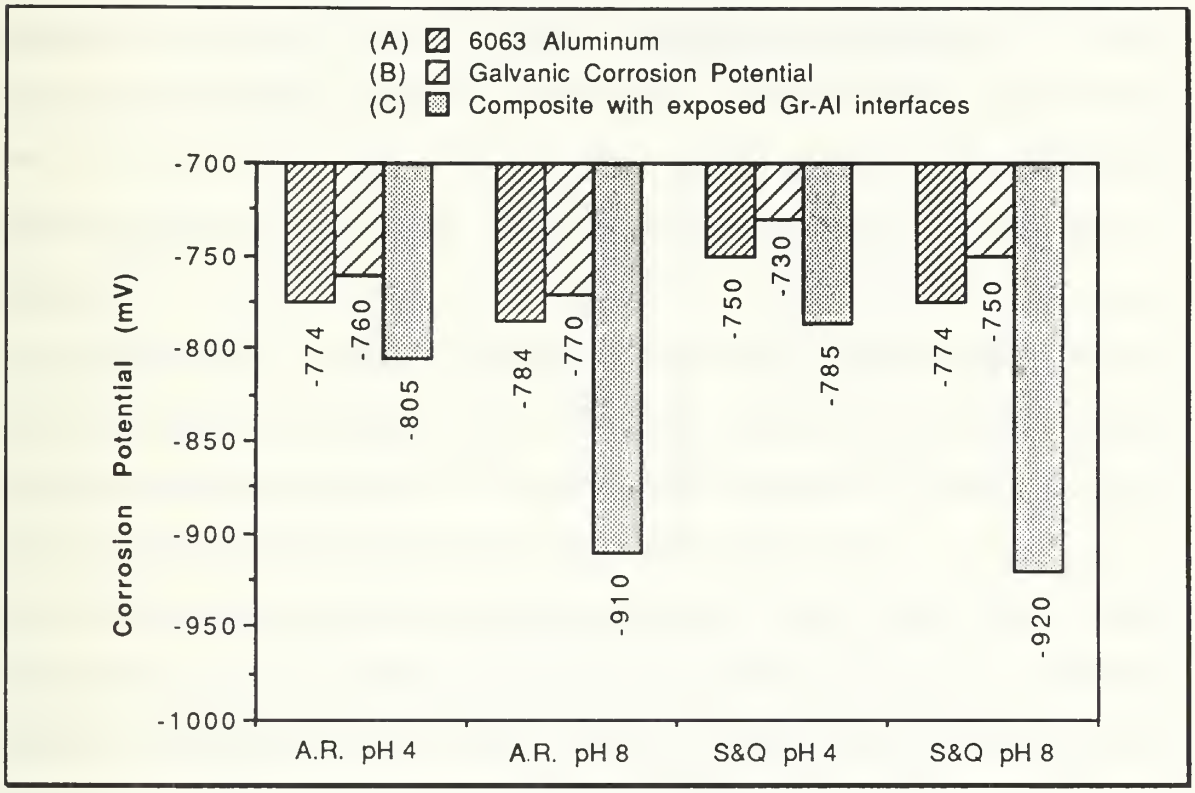

Figure 14: The corrosion potentials of (A), (B), and (C). (B) is polarized electropositively to (A), as anticipated. (C) is electronegative to (A). The behavior of (C) may be due to crevice corrosion, changes in other interfacial corrosion characteristics, or a large local graphite area fraction.

E. IMMERSION TESTS RESULTS

The 22 day duration of the immersion tests was insufficient for any measurable pitting to occur. The immersion coupons were examined under a stereoscopic light microscope (LM). Scanning electron microscopy (SEM) of the coupons was unsuccessful because of charging of the residual oxides.

Accelerated corrosion was noted on the coupons lacking edge protection. The transverse fiber layers, where the fibers ran parallel to the exposed edge, were preferentially attacked. The composite delaminated, swelled, and buckled. The thickness of the coupons increased unevenly from 0.0015 meters to 0.0020 to 0.0025 meters. Using LM corrosion products could be observed interior to the composite where the transverse attack had occurred. This accelerated attack was initially attributed to galvanic coupling between the graphite and aluminum, but the mode of attack cannot be stated with certainty because the corrosion potential of the exposed graphite–aluminum interface is unexpectedly electronegative. The transverse fiber layers presented more interfacial area than the longitudinal layers to the electrolyte, just as the 0.40 area fraction galvanic corrosion tests presented more graphite area than the 0.10 area fraction tests. The area effect may then play role in limiting attack of the longitudinal fiber layers.

Low magnification views of the upper surface foil of the coupons are presented in Figures 15 and 16. Figure 15 was taken prior to the

immersion testing, and Figure 16 was taken after immersion testing. No visible corrosion is evident.

Figures 17 and 18 are representative photographs of the coupons on the immersion racks at the end of the testing, prior to their removal. The limited photographic equipment available necessitated extreme magnification in the dark room when printing. The coupons were respectively with and without edge protection. Note the accumulation of corrosion products on and under the unprotected specimen.

Figures 19 and 20 are representative photomicrographs of the upper surface foil of the composite, prior to and post immersion. No visible corrosion is evident. The irregular appearance is caused by the polishing with 600 grit SiC paper prior to immersion.

Figures 21 and 22 are representative photomicrographs of the exposed edge of a coupon, prior to and after immersion. Note the preferential attack of the transverse graphite fiber layers. No visual difference could be discerned between the edge corrosion at pH 4 and pH 8. This supports the conclusion in the previous section that a mechanism other than galvanic corrosion is operating.

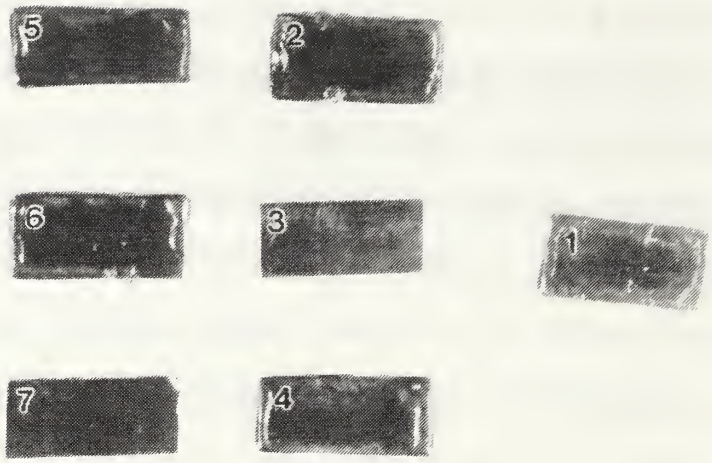

Figure 15: Low magnification view of composite coupons prior to immersion testing.

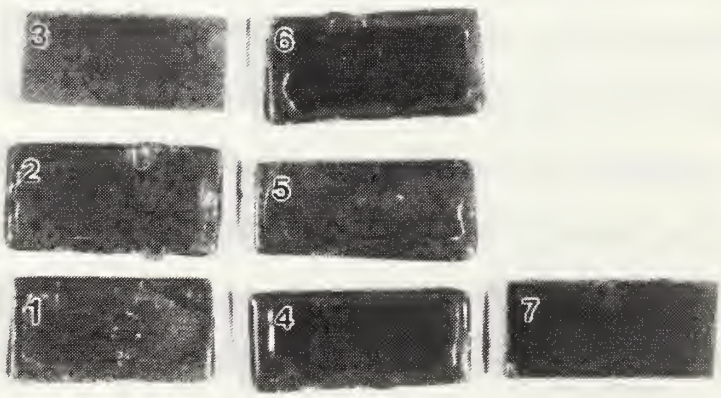

Figure 16: Low magnification view of composite coupons post immersion testing. No pitting is observed.

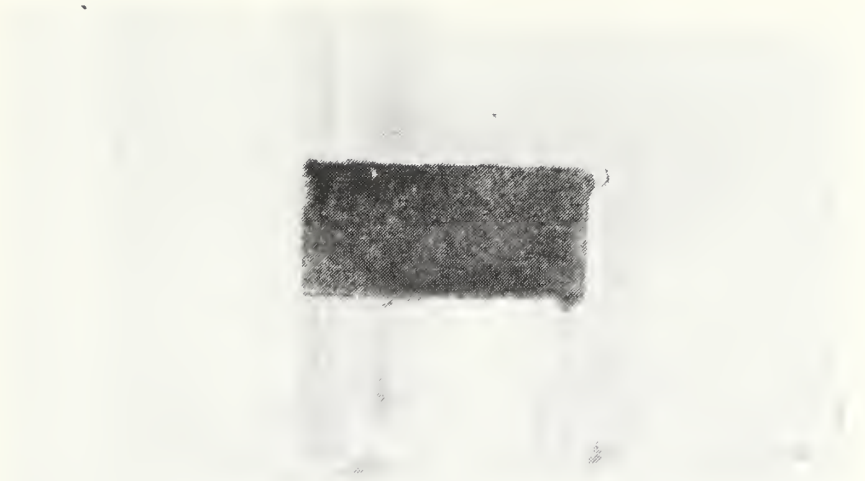

Figure 17: An edge protected immersion coupon in electrolyte at the end of the immersion test. The edge protection has prevented electrolyte access to the graphite–aluminum interface.

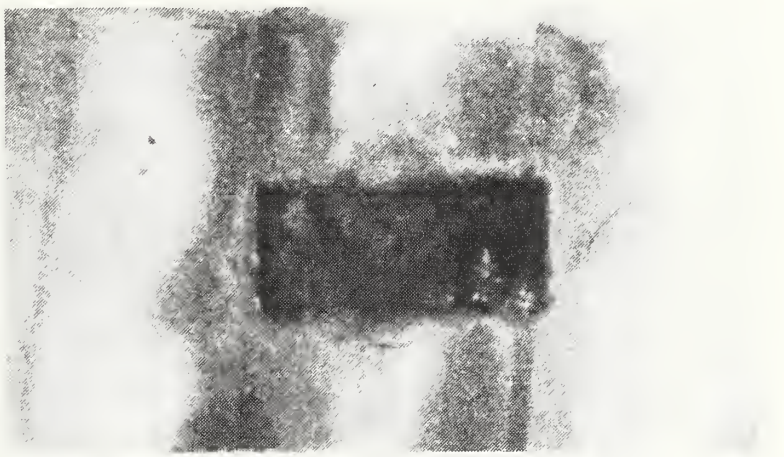

Figure 18: An immersion coupon in electrolyte at the end of the immersion test. The lack of edge protection has allowed electrolyte access to the graphite–aluminum interface, thereby accelerating edge corrosion.

Figure 19: The upper surface of a composite coupon prior to immersion testing. Magnification is 64X.

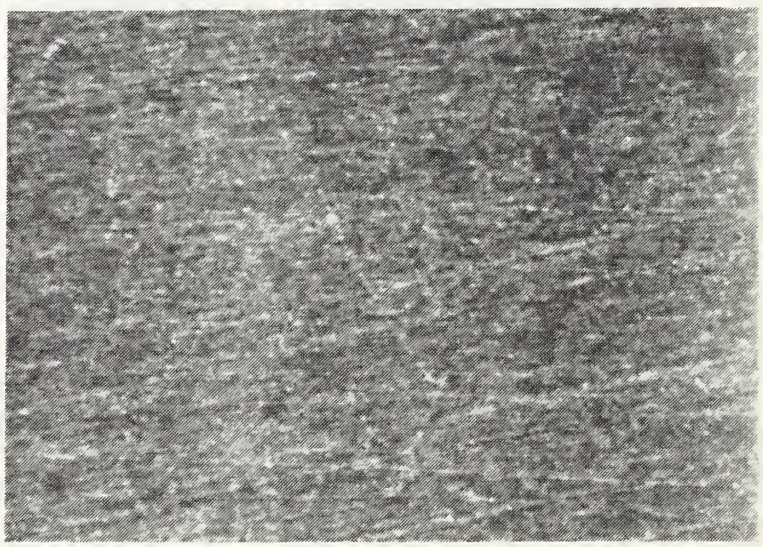

Figure 20: The upper surface of a composite coupon after immersion testing. No pitting is noted. Magnification is 64X.

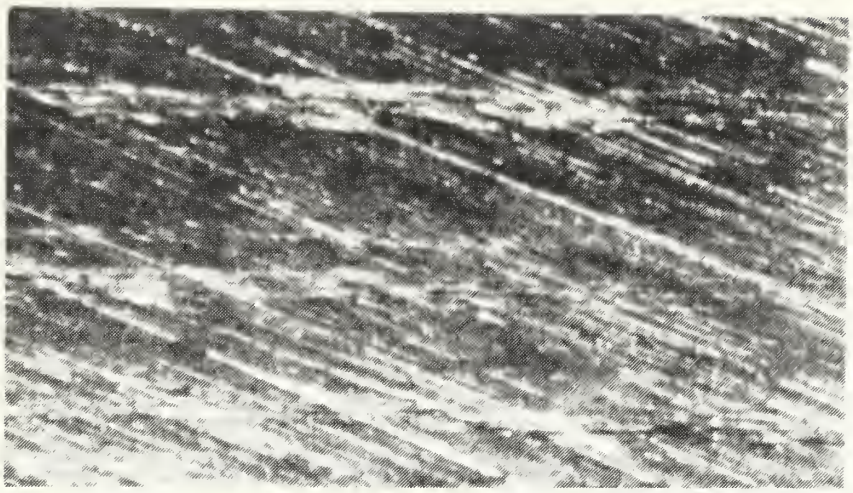

Figure 21: The exposed edge of a composite coupon prior to immersion testing. The edge has been polished with 1 μm diamond dust to emphasize the accelerated corrosion after immersion. Magnification is 64X.

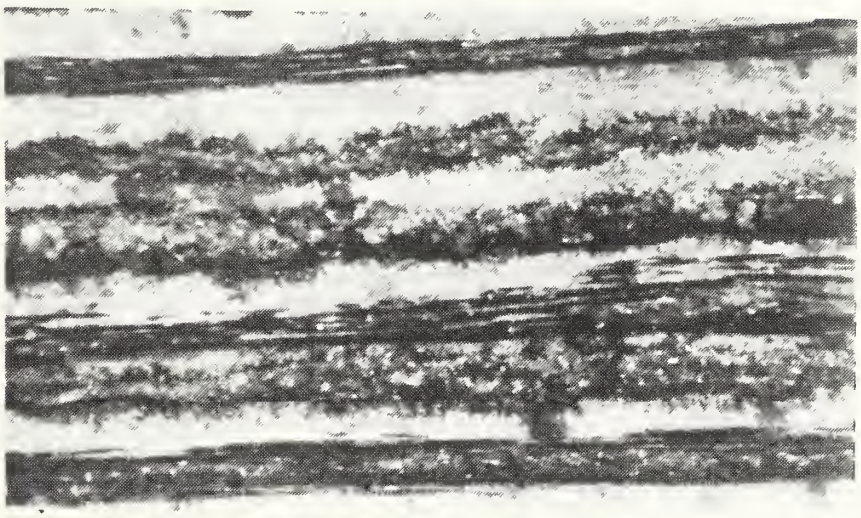

Figure 22: The exposed edge of the composite coupon after immersion testing. Note that the transverse graphite fiber layers were preferentially attacked. Magnification is 64X.

V. CONCLUSIONS

The corrosion behavior of a P-130x graphite fiber reinforced 6063 aluminum metal matrix composite was studied. It was found to be susceptible to several different forms of corrosive attack in 3.5% NaCl aqueous solution. The most vigorous attack occurred at exposed graphite-aluminum interfaces. Immersion tests showed accelerated corrosion at the exposed interfaces, with preferential attack at transverse fiber layers.

At first it was believed that this was due to galvanic coupling of the graphite and aluminum. The galvanic corrosion tests measured a galvanic current several times that of the i_{corr} determined from linear polarization. Current flow was greater at pH 4 than pH 8. This was attributed to a change in the oxygen reduction reaction occurring at the cathode. As the exposed area fraction increased, corrosion current increased. This was attributed to the area effect. The common galvanic potential of the electrically shorted galvanic couple was electropositive to the general corrosion potential of the monolith, indicating that the graphite was polarizing the aluminum electropositively, as expected. Solutionizing and quenching the metal electrode yielded a lower corrosion current than when the electrode was in the T1 temper, for reasons not fully understood.

The electrochemical methods used to study pitting reveal only thermodynamic tendencies, and not kinetics. Immersion testing in

unbuffered solutions was performed to study the pitting kinetics, but the length of the run was insufficient to conclusively show pitting. Some pitting research documented in the literature ran over a period of years [Ref. 11] [Ref. 18] [Ref. 25]. The results of the corrosion potential and galvanostaircase measurements of repassivation potential indicate that the composite in the as received state is susceptible to pitting. Solutionizing and quenching the composite increased its pitting susceptibility at pH 4, and conferred pitting immunity at pH 8. As naturally occurring sea-water is a moderately buffered solution with an approximate pH of 8, this is an important finding.

The corrosion current for pH 4 was found to be greater than that at pH 8, as expected on the basis of a changing cathodic half-cell reaction. For the most part, the corrosion current for the as received condition was greater than that for the solutionized and quenched state. The corrosion current for the monolith was greater than that of the composite's surface foil. This is tentatively attributed to a differing thermomechanical processing history and/or differing actual compositions. The presence of the sulfite ion increased the corrosion current. This is attributed to the oxidizing power of SO_3^{2-}.

When the corrosion potential of a composite sample abraded to expose the the interfaces was found to be electronegative to the corrosion potential of the monolith, the view that this accelerated corrosion was classical galvanic coupling was thrown into doubt. This result may be due to preferential crevice attack of the interface, changes in other interfacial corrosion characteristics which are not

yet understood, or unusually high local graphite area ratios. Immersion tests show preferential attack at transverse fiber layers, which may be due to the area effect, or may be a crevice corrosion phenomena.

General corrosion currents were much lower than galvanic corrosion currents. Although the accelerated corrosion observed at the edges of the composite during the immersion test does not appear to be classic galvanic corrosion, its rate was much faster than either pitting or general corrosion. If the edges of the composite are protected from the electrolyte while in service, accelerated corrosion will not occur until localized corrosion perforates the composite's surface foil.

VI. RECOMMENDATIONS FOR FUTURE RESEARCH

A series of buffered electrochemical measurements using increasing concentrations of the sulfite ion might better elucidate the effect of the ion upon corrosion of the metal–matrix composite. These tests should include galvanic corrosion measurements, measurement of the corrosion potential, determination of the repassivation potential through galvanostaircase polarization, and calculating corrosion current using linear polarization.

The length of the immersion tests was insufficient to allow correlation with the electrochemical pitting susceptibility measurements. While one approach might be to increase the length of the runs, scribing a standardized scratch upon the immersion coupon would speed localized corrosion initiation. Quantitative measurements of the scratch depth and width after a three–week immersion might yield the desired correlation.

Considering the coastal positioning of the Naval Postgraduate School, longer term immersion tests could easily be performed in the Pacific. Several months may be required for results, so this may best be started by one graduate student and finished by a second.

Thermomechanically processing monolithic 6063 aluminum to the state of the foils of the metal matrix composite may yield specimens whose electrochemical measurements would explain the anomaly of the abraded composite's corrosion potential. Building up a carbide layer on the galvanic current's metal electrode by solutionizing in the

presence of carbon could further simulate the aluminum-graphite interface.

The intense galvanic corrosion observed at and interior to the edge of the composite may be modeled by conducting galvanic corrosion experiments in a deaerated, low pH, high chloride ion concentration electrolyte. The effect of heat treatments and the presence of the sulfite ion on these results would indicate their environmental influence on corrosion propagation interior to the composite once the outer surface foil is perforated or edge protection defeated.

A more complex galvanic experiment would involve two chambers linked by a salt bridge. Pitting involves anodic and cathodic reactions within differing environments. The anodic environment within the pit is of low pH, deaerated, and has a high chlorine ion concentration. The cathodic environment on the open surface of the metal is the ambient environment. One chamber would simulate the anodic environment, the second the cathodic. The salt bridge would allow the ionic flow necessary to galvanic corrosion. Various combinations of aluminum, aluminum-carbide, and graphite electrodes could be utilized to simulate the pitting potentials measured.

Galvanic corrosion experiments should be performed using large graphite area fractions, to determine if an unusually large graphite area fraction could electronegatively polarize the galvanic couple with respect to the general corrosion potential of the monolithic matrix metal.

APPENDIX A

Relationship between Corrosion Rate and Corrosion Current

Once a value of i_{corr} has been determined, corrosion rate calculations may be made using Faraday's Law, which states that the amount of material converted in an electrochemical reaction is proportional to the current passed in the reaction.

$$W = (\frac{A}{ZF}) \bullet (I \bullet t)$$

where:

- W = weight reacted
- A = atomic weight
- Z = number of equivalents per mole
- F = Faraday's constant (96,500 coulombs)
- I = measured current
- t = measured time.

Dividing both sides of the equation by time and surface area, we arrive at a measure of the rate of weight loss (w) in terms of the current density (i).

$$w = \frac{A}{ZF} \bullet i$$

The weight loss rate is commonly expressed in milligram per decimeter squared per day. Now by dividing both sides of the equation by the density (ρ) the rate of penetration (r) is obtained. [Ref. 17:pp. VII 13-28]

$$r = \frac{w}{\rho} = \frac{A}{\rho ZF} \bullet i$$

APPENDIX B

Derivation of Corrosion Current from L–P Plots and Tafel Slopes

At E_{corr}, an externally measured current (i_{meas}) would be found to be zero, as the currents resulting from the oxidation reactions (i_o) and the reduction reactions (i_r) would be equal.

$$i_{corr} = i_o - i_r = 0 \quad \text{at } E_{corr}$$

Impressing an overvoltage, the electrode will develop a measurable external current:

$$i_{meas} = i_o - i_r \neq 0$$

The overvoltage (η), which is the difference between the applied potential (E_{app}) and E_{corr}, is related to i_o and i_r by the Tafel equations as follows:

$$\eta = \beta_a \log \frac{i_o}{i_{corr}} \qquad (1)$$

$$\eta = -\beta_c \log \frac{i_r}{i_{corr}} \qquad (2)$$

Where $\eta = E_{app} - E_{corr}$, and β_a and β_c are the Tafel constants for the anodic and cathodic legs of polarization. Dividing both sides of

Equations 1 and 2 by the appropriate Tafel constant, and then taking the inverse base ten logarithm, we obtain:

$$\log \frac{i_o}{i_{corr}} = \frac{\eta}{\beta_a} \quad \text{or} \quad 10^{\eta/\beta_a} = \frac{i_o}{i_{corr}}$$

$$\log \frac{i_r}{i_{corr}} = -\frac{\eta}{\beta_c} \quad \text{or} \quad 10^{-\eta/\beta_c} = \frac{i_r}{i_{corr}}$$

$$i_{corr} = i_o - i_r = i_{corr} (10^{\eta/\beta_a} - 10^{-\eta/\beta_c})$$

The power function 10^x may be approximated by the power series

$$10^x = 1 + 2.3x + \frac{(2.3x)^2}{2!} + \ldots + \frac{(2.3x)^n}{n!} + \ldots$$

If x is small, the third and higher terms may be neglected without significant error. Substituting η/β_a and $-\eta/\beta_c$ for x gives

$$10^{\eta/\beta_a} = 1 + 2.3 (\eta/\beta_a)$$

$$10^{-\eta/\beta_c} = 1 - 2.3 (\eta/\beta_c)$$

Substituting and simplifying yields

$$i_{meas} = 2.3\, i_{corr}\, \eta\, \frac{\beta_a + \beta_c}{\beta_a\, \beta_c}$$

Bearing in mind that η/i_{meas} is the slope (S) of the linear region of the polarization resistance, further manipulation gives the final result of:

$$\eta / i_{meas} = S = \frac{\beta_a \beta_c}{2.3\, i_{corr} (\beta_a + \beta_c)}$$

$$i_{corr} = \frac{\beta_a \beta_c}{2.3\, S (\beta_a + \beta_c)}$$

For the higher order terms in the power series to have been neglected, it was necessary to specify a small η/β. For a typical value of β of 100 mV/Decade, η should be less than 10 mV.
[Ref. 17:pp. VII 29-37]

APPENDIX C

Determination of Fiber Length for Galvanic Corrosion Experiments

Assuming a circular cross section of the fibers, with complete electrolyte access, and neglecting the area at the ends of the fibers, the length of tow necessary for graphite area fractions of 0.10 and 0.40 may be calculated.

First, the surface area per m length of a two–thousand fiber tow of 10μm diameter graphite fibers was calculated to be:

$$a_G = N\pi D$$

where:

- a_G = Graphite Area per m length
- N = Number of fibers in the tow (2000)
- D = Diameter (10 μm)

Next, the length of tow necessary such that some fraction of the total working surface area was graphite was calculated to be:

$$X = \frac{La_G}{La_G + A_m}$$

$$X\,(La_G + A_m) = La_G$$

$$La_G\,(1 - X) = XA_m$$

$$L = \frac{XA_m}{a_G (1 - X)}$$

$$L = \frac{XA_m}{N\pi D (1 - X)}$$

where:

- A_m = Metal Area (0.0008 m^2)
- X = Area Ratio or Fraction
- L = Length of Tow (m)

For an area fraction of 0.10, the length of graphite tow required was:

$$L = \frac{(0.1)\ (0.0008)}{(2000)\ (\pi)\ (10^{-6})\ (0.9)} = 0.00141 \text{ m}$$

And for the 0.40 area fraction:

$$L = \frac{(0.4)\ (0.0008)}{(2000)\ (\pi)\ (10^{-6})\ (0.6)} = 0.00849 \text{ m}$$

Two graphite fiber electrodes were constructed as described earlier, one with an exposed fiber length of 0.0014 m, and the second with an exposed fiber length of 0.0085 m.

REFERENCES

1. Kreider, K. G., in *Introduction to Metal-Matrix Composites*, Kreider, K. G., ed., pp. 1-8, Academic Press, 1974.

2. MMIAC, *Introduction to Metal Matrix Material*, MMCIAC #272, p. 2-2, 1982.

3. Bonewitz, R. A., "An Electrochemical Evaluation of 1100, 5052, and 6063 Aluminum Alloys for Desalination," *Corrosion*, Vol. 29, pp. 215-222, June 1973.

4. Materials Advisory Group U.S. Army Material Command and NACE, Paper No. 29, *Corrosion of Electronic Equipment Aboard Naval Ships*, Bjelland, L. K., and Schuler, M. D., pp. 387-388, December 1972.

5. Shreir, L. L., *Corrosion Volume 1 Metal/Environment Reactions*, p. 4:16, Newnes-Butterworths, 1976.

6. Fontana, M. G., *Corrosion Engineering*, pp. 63-73, McGraw-Hill, 1986.

7. Trzaskoma, P. P., "Aqueous Corrosion of Metal-Matrix Composites," *Journal of Metals*, Vol. 40, pp. 21-23, December 1988.

8. Vassilaros, M. G., and others, in *Mechanical Behavior of Metal-Matrix Composites*, Hack, J. E., and Amateau, M. F., eds., pp. 335-353, TMS-AIME, 1983.

9. Pfeifer, W. H., in *Hybrid and Select Metal Matrix Composites: A State-of-the-Art Review*, Renton, W. J., ed., pp. 231-255, American Institute of Aeronautics and Astronautics, 1977.

10. Metzger, M., and Fishman, S. G., "Corrosion of Aluminum–Matrix Composites. Status Report," *Industrial Engineering Chemistry Product Resources Development*, Vol. 22, pp. 296-302, June 1983.

11. Aylor, D. M., and Moran, P. J., "Effect of Reinforcement on the Pitting Behavior of Aluminum–Base Metal Matrix Composites," *Journal of the Electrochemical Society: Electrochemical Science and Technology*, Vol. 132, pp. 1277-1281, June 1985.

12. Aylor, D. M., and Moran, P. J., "Pitting Corrosion Behavior of 6061 Aluminum Foils in Sea Water," *Journal of the Electrochemical Society: Electrochemical Science and Technology*, Vol. 133, pp. 949-951, May 1986.

13. American Society for Testing and Materials, ASTM Special Technical Publication 864, *Recent Advances in Composites in the United States and Japan*, Aylor, D. M., and Kain, R. M., pp. 632-647, June 1983.

14. Sedriks, A. J., Green, J. A. S., and Novak, D. L., "Corrosion Behavior of Aluminum–Boron Composites in Aqueous Chloride Solutions," *Metallurgical Transactions*, Vol. 2, pp. 871–875, March 1971.

15. Pohlman, S. L., "Corrosion and Electrochemical Behavior of Boron/Aluminum Composites," *Corrosion*, Vol. 34, pp. 156-159, May 1978.

16. Maruyama, B., and Rabenberg, L., in *Interfaces in Metal–Matrix Composites*, Dhingra, A. K., and Fishman, S. G., eds., pp. 233-239, TMS–AIME, 1986.

17. EG&G Princeton Applied Research, *Model 351 Corrosion Measurement System Preliminary Operating Manual*, 1985.

18. Wilde, B. E., "A Critical Appraisal of Some Popular Laboratory Electrochemical Tests for Predicting the Localized Corrosion Resistance of Stainless Alloys in Sea Water," *Corrosion*, Vol. 28, pp. 282-291, August 1972.

19. Wilde, B. E., and Williams, E., "On the Correspondence between Electrochemical and Chemical Accelerated Pitting Corrosion Tests," *Journal of the Electrochemical Society : Electrochemical Science*, Vol. 117, pp. 775-779, June 1970.

20. Aylor, D. M., and Moran, P. J., "The Influence of Incubation Time on the Passive Film Breakdown of Aluminum Alloys in Sea Water," *Journal of the Electrochemical Society : Electrochemical Science and Technology*, Vol. 133, pp. 868-872, May 1986.

21. Hirozawa, S. T., "Galvanostaircase Polarization", *Journal of the Electrochemical Society : Electrochemical Science and Technology*, Vol. 130, pp. 1718-1721, August 1983.

22. American Society for Testing and Materials, "Standard Test Method for Conducting Cyclic Potentiodynamic Polarization Measurements for Localized Corrosion Susceptibility of Iron-, Nickel-, or Cobalt-Based Alloys," Designation: G 61-86, *Annual Book of ASTM Standards*, pp. 229-232, 1989.

23. American Society for Testing and Materials, "Standard Test Method for Conducting Cyclic Galvanostaircase Polarization," Designation: G 100-89, *Annual Book of ASTM Standards*, pp. 260-262, 1989.

24. EG&G Princeton Applied Research, *Model K47 Corrosion Cell System Operating and Service Manual*, 1980.

25. Wilde, B. E., and Williams, E., "The Relevance of Accelerated Electrochemical Pittings Tests to the Long-Term Pitting and Crevice Corrosion Behavior of Stainless Steels in Marine Environments," *Journal of Electrochemical Society: Electrochemical Science*, Vol. 118, pp. 1057-1062, July 1971.

INITIAL DISTRIBUTION LIST

		No. Copies
1.	Defense Technical Information Center Cameron Station Alexandria, VA 22304-6145	2
2.	Library, Code 0142 Naval Postgraduate School Monterey, CA 93943-5002	2
3.	Professor I. Dutta Code 69Du Department of Mechanical Engineering Naval Postgraduate School Monterey, CA 93943	3
4.	Naval Engineering Curricular Office Code 34 Naval Postgraduate School Monterey, CA 93943	1
5.	LT Joel D. King, USN 143 Howell Dr. Somerville, NJ 08876	1
6.	Mr. Kevin G. Beasley Electronic Development Department Naval Weapons Support Center Crane, IN 47522	1
7.	Dr. Patricia P. Trzaskoma Surface Protection Section Code 6322 Material Science and Technology Division Naval Research Laboratory Washington, DC 20375	1

617-586

Thesis
K435 King
c.1 Characterization of the corrosion of a P-130x graphite fiber reinforced 6063 aluminum metal matrix composite.

Thesis
K435 King
c.1 Characterization of the corrosion of a P-130x graphite fiber reinforced 6063 aluminum metal matrix composite.

AMERICAN BINDERY TOPEKA, KANSAS

thesK435
Characterization of the corrosion of a P
3 2768 000 89658 3
DUDLEY KNOX LIBRARY